NASA TECHNICAL NOTE

NASA TN D-5029

c. 1

FULL-SCALE DYNAMIC LANDING-IMPACT INVESTIGATION OF A PROTOTYPE LUNAR MODULE LANDING GEAR

by Ulysse J. Blanchard

Langley Research Center
Langley Station, Hampton, Va.

FULL-SCALE DYNAMIC LANDING-IMPACT INVESTIGATION

OF A PROTOTYPE LUNAR MODULE LANDING GEAR

By Ulysse J. Blanchard

Langley Research Center
Langley Station, Hampton, Va.

Technical Film Supplement L-1011 available on request.

NATIONAL AERONAUTICS AND SPACE ADMINISTRATION

FULL-SCALE DYNAMIC LANDING-IMPACT INVESTIGATION
OF A PROTOTYPE LUNAR MODULE LANDING GEAR

By Ulysse J. Blanchard
Langley Research Center

SUMMARY

In order to subject prototype components of a lunar-module (LM) landing gear to some of the dynamic loads of lunar-landing impact, full-scale tests were conducted at simulated lunar gravity. The full-scale tests were conducted with a planar (three degrees of freedom) lunar-gravity simulator and a full-scale test vehicle. Structural integrity of a prototype landing-gear system (struts and deployment trusses) was substantiated. Dynamic performance of the landing-gear struts was good for all landing conditions tested including those which produced near maximum strokes and loads. Theoretical results were in agreement with experimental results obtained for landing accelerations, gear forces and strokes, and vehicle pitch motions.

INTRODUCTION

The LM lunar landing operation is one of the critical phases of the Apollo mission of placing a manned spacecraft on the lunar surface and returning the crew to earth. Landing impact is of particular concern because the landing-gear system must provide required shock attenuation and must maintain structural integrity in order to assure stability against overturning and prevent damage which would jeopardize postlanding launch operations. Prior to an actual landing mission, dynamic proof tests of prototype landing-gear components are desirable. This paper presents results of a full-scale dynamic landing-impact investigation of an LM prototype landing-gear system.

The experimental investigation was conducted at Langley Research Center (LRC) with an existing lunar-gravity impact simulator and a full-scale test vehicle which had been previously used for technique evaluation tests described in reference 1. The lunar-gravity simulator made it possible to proof test the complete landing-gear system under dynamic impact loads and motions similar to those which may occur in a lunar landing. The cable-supported vehicle and the inclined landing surface were suitable for conducting landing tests which involved planar (three degrees of freedom) motions. Landings were made at selected initial conditions to investigate maximum loading and stroking of the

landing-gear struts and to induce post-touchdown motions which provided some stability data.

In the present paper, experimental results from 21 landings with the prototype landing gear are shown. Vehicle motions, accelerations, and landing-gear forces and strokes are presented. Comparisons are also presented between these experimental results and theoretical results obtained by the NASA Manned Spacecraft Center (MSC). An unpublished theoretical analysis entitled "MSC Lunar Module Landing Program" was used by the Landing and Docking Mechanics Branch of Manned Spacecraft Center to obtain the theoretical results.

SYMBOLS

The units used for the physical quantities defined in this paper are given both in U.S. Customary Units and in the International System of Units (SI). (See ref. 2.) Appendix A presents factors relating these two systems.

g	acceleration due to earth gravity, 32.2 ft/sec^2 (9.81 m/s^2)
C	compression stroke
C_1	compression stroke, first stage
C_2	compression stroke, second stage
T	tension stroke
T_1	tension stroke, first stage
T_2	tension stroke, second stage
V_h	horizontal velocity, ft/sec (m/s)
V_v	vertical velocity, ft/sec (m/s)
X, Y, Z	body axes

2

DESCRIPTION OF TEST VEHICLE

The full-scale test vehicle of reference 1 which was modified for the present landing investigation is shown in figure 1. Pertinent characteristics are given in table I. The outrigger trusses were modified in order to permit installation of four prototype landing-gear structures. Ballast mass was redistributed in order to duplicate updated mass and inertial properties of the LM. The test-vehicle body did not duplicate the elastic characteristics of the prototype LM body. Since all mass was used for ballast and structure, the test vehicle body was both stronger and less flexible than the prototype. Duplicating prototype body structural characteristics was not considered necessary for the main purpose of the present investigation.

Landing Gear

The prototype landing-gear components tested and shown in figure 2 included primary and secondary shock-absorbing struts and deployment trusses. The arrangement shown is referred to as the "cantilever" gear. Strut and truss details are shown in figures 3 and 4, respectively. Pertinent landing-gear characteristics are also given in table I. The landing gear was designed and constructed by the contractor and provided by Manned Spacecraft Center for these tests. The landing gear is a typical prototype structure since subsequent and continuing refinements are being made in order to reduce weight.

Each of the four landing-gear assemblies (fig. 2) consists of a primary strut (with a footpad at its lower end), two secondary struts, and a deployment truss. The landing gear was constructed of high-strength aluminum alloys (2024, 7075, and 7079) and titanium alloys. All aluminum parts were anodized. In addition, sliding surfaces were plated with a dry lubricant. The sliding coefficient of friction of the primary-strut bearings, as determined from static bench tests, was approximately 0.3 for the present landing tests. The footpad used for the present test was not a prototype article but a special "boilerplate" pad used to vary landing surface-pad interface conditions.

The primary strut (fig. 3(a)) consists of a telescoping inner cylinder, an outer cylinder connected through a universal joint at its upper end to the outrigger truss, and a crushable aluminum honeycomb cartridge to absorb impact energy. Each secondary strut (fig. 3(b)) consists of an outer cylinder connected by a ball-socket joint to the outer cylinder of the primary strut, a sliding inner cylinder connected by a universal joint to the deployment truss, and an arrangement of crushable honeycomb cartridges that can absorb

energy while the double-acting secondary strut is lengthening or shortening. The mechanical design of the secondary strut provides for compression crushing of different honeycomb cartridges during the tension (lengthening) and compression (shortening) strokes of the double-acting strut. All struts were vented to minimize air entrapment.

The gear deployment truss (fig. 4) was tested in the gear-down position as part of the total landing-gear structure. The gear-down lock of the truss was engaged and pinned in this position. Actuator springs and mechanisms were not included as part of these tests.

Shock Absorbers

The energy-absorbing cartridges contained within the landing-gear struts are shown in figure 5 before and after impact crush. The cartridge assemblies comprise crushable-aluminum-honeycomb cylinders, stage-separator plates, and strut-assembly end plates. When a design compression load is applied to the honeycomb cylinders, a progressive local-buckling failure (crush) occurs. This condition produces a constant crush-force level during the strut stroke which serves to absorb the vehicle-impact energy and limit loads imposed on the vehicle and landing-gear structure. Shock-absorber force staging was accomplished by stacking honeycomb elements of different crush strengths in a single cartridge.

The honeycomb cylinders were fabricated, precrushed, and certified by the vendor for static-crush-force levels specified in table I. More stringent honeycomb crush-force tolerances than the ±5 percent specified in table I can be achieved with associated increase in unit cost. However, for the purpose of the present investigation, the subject material was considered to be adequate. The honeycomb was intentionally procured at static crush-force levels about 10 percent lower than the design dynamic crush force desired (table I) in order to compensate for a strain-rate effect which causes an increase in the crush-force level of aluminum honeycomb. The cartridge elements were assembled and bonded into units at LRC.

APPARATUS AND PROCEDURE

The full-scale tests were conducted on a planar (three degrees of freedom) lunar-gravity impact simulator located at the Langley lunar landing research facility. The lunar-gravity simulator, described in reference 1 and shown in figure 6, consisted of an inclined-plane landing surface, an overhead trolley and track, and a fixed-length cable which supported the test vehicle from the overhead trolley in a near-horizontal position on the landing surface. Lunar gravity was obtained by displacing the vehicle (fig. 6(b)) from directly beneath the overhead trolley so that the force exerted statically by the

vehicle on the landing surface was equal to its lunar weight. Another system of cables and winches, described in detail in reference 1, was used to position and release the vehicle as a deflected pendulum, gravity imparting the desired landing speeds at impact upon the landing surface.

Test Conditions

A sketch identifying vehicle axes, accelerations, attitudes, velocity vectors, and landing-gear orientation during landing is presented in figure 7. The initial landing conditions for each of the 21 landings are listed in table II. The touchdown pitch attitudes and speeds were obtained from motion-picture film. The cartridge static crush forces listed in table II are the average values of all like elements randomly installed in all gears prior to each landing. Two symmetric landing-gear orientations were used for the present tests: two gear legs leading with two legs trailing (2-2 orientation), and one gear leg leading with one leg trailing (1-2-1 orientation). The test vehicle was landed with positive and negative pitch attitude and at some speeds higher than that specified for LM guidance and control capability in order to attain desired gear stroke, load, and vehicle motions. This type of landing was necessary since the range of possible vehicle orientations and landing-surface conditions was limited by the planar constraints of the simulator. Landing-surface—pad interface conditions were varied by allowing the foot-pads to slide at different values of sliding coefficient of friction or by constraining the pads (coefficient of friction, ∞) at impact with sharp spikes installed on the bottom of the pads. Landing-surface depressions or slopes were simulated by placing elevated platforms 2 feet (0.61 m) high at the impact location for selected pads. In general, the landing conditions were selected to induce loading conditions which would involve high bearing-friction loads on the primary struts and near full stroking for various stroking phases of all the struts. Five consecutive landings were made at a single set of launch conditions (landings 11 to 15) in order to determine repeatability with regard to initial impact conditions, landing dynamics, and performance of a single gear during repeated near maximum loading and stroking. A few landings were made at conditions which produced pronounced rocking motions in order to provide some stability data.

All tests were conducted outdoors at ambient conditions from mid-summer to mid-winter. The landing gears were exposed to normal atmospheric contamination, temperature, and ground-level winds. The shock-absorbing struts were checked during tests for visible signs of contamination and were kept indoors as much as possible between landings; however, some exposure was unavoidable.

Instruments and Measurements

Landing-impact accelerations were measured at the vehicle center of gravity with 50g linear servo accelerometers rigidly mounted on a platform attached to the lower face of the large lead-filled counterweight. The accelerometers were alined so that the accelerations were measured in the plane of the horizontal velocity vector V_h for both 2-2 and 1-2-1 landing orientation. The accelerometers which had natural frequencies of approximately 650 cycles per second (650 Hz) were used to measure normal, longitudinal, and angular accelerations. They were damped to about 65 percent of critical damping. Angular acceleration was measured by coupling a pair of the linear accelerometers which had been adjusted so that their response and phase characteristics were matched. The response of the recording oscillograph galvanometers was flat to 24 cycles per second (24 Hz) for the angular and longitudinal accelerometers. Signals of the normal accelerometer were fed through two recording galvanometers, one having a flat response to 24 cycles per second (24 Hz) and the other to 120 cycles per second (120 Hz).

Axial forces generated during stroking of the landing-gear struts were measured with resistance-wire strain gages. The gages were installed at the lower end of the inner cylinders of the four primary struts and on the deployment-truss connection fittings of the eight secondary struts. The stroking force measured by the strain gages was the sum of the force reacted by the honeycomb cartridge and the force reacted by bearing friction. Primary-strut axial forces resulting from secondary strut vector components acting on the outer cylinder were not measured. Response of the recording oscillograph galvanometers was 240 to 360 cycles per second (240 to 360 Hz). Total strut strokes were obtained by measuring the honeycomb-cartridge lengths before and after each landing.

Landing impacts were observed and were also recorded by motion-picture cameras located at the overhead track. Motion pictures (taken at 24, 64, and 200 frames per second) and a background grid were used to determine vehicle landing speeds, pitch attitude, and pitch-motion time histories during landing impact.

RESULTS AND DISCUSSION

Experimental landing-gear force and stroke, vehicle acceleration, and pitch-motion data are presented. Accelerations are expressed in units of earth gravity. These experimental data are also compared with theoretical results obtained from computer-simulated landings. The geometry and mass-inertia properties of table I; initial landing-impact conditions and average honeycomb static crush forces of table II; and modifying effects such as honeycomb strain rate, strut-bearing friction, and viscous damping were used in the theoretical model of the full-scale test vehicle.

6

A motion-picture supplement (L-1011) showing the tests discussed in this paper has been prepared and is available on loan. A request card form and a description of the film are included at the back of this paper.

Landing-Gear Forces

The axial stroking forces measured during honeycomb crush on each of the secondary and primary struts of the four landing gears for all landings are presented in table III and plotted in figures 8 and 9, respectively. The data points are the faired value of the force time histories obtained during dynamic crushing of each honeycomb-cartridge stage and includes strut-bearing friction and possibly some pumping due to entrapped air. The dashed-line curves of figures 8 and 9 indicate the predetermined static crush-force range (nominal ±5 percent) of the corresponding honeycomb cartridge stages.

In the case of the secondary struts (fig. 8), the average of the strut forces measured for all the landings was very near the nominal honeycomb design dynamic crush force (solid line), 4500 lbf (20 kN) for the compression stroke and 500 and 5000 lbf (2 and 22 kN) for the first and second stages of the tension stroke, respectively. The secondary struts are only loaded axially and the friction forces are small; therefore, the increase in measured force over the honeycomb static force is primarily due to dynamic (strain-rate) effects. The data indicate that the honeycomb shock absorbers and the struts were performing according to design.

The axial stroking forces measured on the primary struts during landings are shown in figure 9. Unlike the secondary struts, the primary struts can be loaded transversely (by the secondary struts) as well as axially. Because of the cantilever design of the primary-strut inner cylinder, these transverse loads can result in significant bearing-friction forces in addition to the honeycomb crush force during the strut stroke. The magnitude of the bearing-friction forces is dependent upon landing orientation and attitude, strut-stroke sequence and phasing, and landing-surface conditions. In most cases the measured stroking forces shown in figure 9 are higher than the honeycomb design dynamic crush values (solid lines) of 4500 and 9500 lbf (20 and 42 kN). For landings at positive pitch attitude (unflagged symbols), this increase is more pronounced during crushing of the first-stage elements of the honeycomb cartridges. One of the contributing factors is that during the first-stage portion of the stroke, the longer cantilevered length of the strut inner cylinder results in larger bending moments and associated higher bearing-friction forces. During first-stage stroking in the case of 1-2-1 landings (fig. 9(b)), forces measured on landing gear 1 were approximately 50 percent greater than those for the honeycomb-design dynamic crush level. Forces were not obtained for landing gear 3 because of instrument failure; however, they should have been about the same as those for landing gear 1. In this landing configuration, the primary struts

of gears 1 and 3 (side gears) stroked very little and were at the maximum cantilevered condition with large transverse loads acting. The flagged data (fig. 9(a)) are for landings at negative pitch attitude and they exhibit similar characteristics with even greater bearing friction force evident than for landings at positive pitch attitudes.

Landing number 16 (fig. 9(b)) was made to obtain large secondary-strut tension strokes and to impose large bending moments on the primary struts. The landing was made with vertical speed only and with gears 2 and 4 impacting on raised platforms. In addition, the gear footpads were allowed to slide outward. The coefficient of surface-pad friction for this landing was about 0.4. The landing energy was absorbed by substantial stroking of both the primary and secondary struts of gears 2 and 4. The maximum primary-strut stroking force measured during all the tests (12,500 lbf (56 kN)) was obtained during this landing. For the next landing (number 17), the coefficient of friction was reduced further to about 0.15 in order to allow the pads to slide more freely. As a result, practically all the impact energy was absorbed by near-maximum tension stroking of the secondary struts of gears 2 and 4. The primary struts did not stroke or develop significant axial loads; however, it was evident from motion pictures that high bending loads occurred in primary struts 2 and 4. No failures occurred and the struts subsequently functioned normally.

During the varied and repeated loadings of the present tests, the four prototype landing gears performed as designed and no structural deficiencies were noted. The variable bearing-friction force in the primary struts was not a problem during these tests and, in general, the force pulses generated were similar to the constant-force characteristics of crushable aluminum honeycomb. Strut-force characteristics were repeatable. The structural integrity of the landing gear, designed for a single landing cycle on the lunar surface, was substantiated.

Comparisons of theoretical strut stroking forces with the experimental values of the present investigation are shown in figures 10 and 11. Typical stroking-force time histories are compared in figure 10. Figure 10(a) shows a typical 2-2 landing at positive pitch attitude, figure 10(b) shows a 2-2 landing at negative pitch attitude, and figure 10(c) shows a 1-2-1 landing. There is good agreement between experimental and theoretical time histories. The stroking forces experienced during each landing by each of the corresponding struts of the full-scale vehicle and the theoretical model are plotted as abscissa and ordinate, respectively, in figure 11. The first-stage tension-stroke force data for the secondary struts are not shown since their magnitudes were small. The solid line (1:1 slope) represents exact agreement. Close agreement was found between experimental and theoretical results. The stroking forces (applied forces) are an important factor in the landing dynamics, and the correlation between measured and predicted forces is a strong indication of the validity of the theoretical analysis.

Landing-Gear Stroke

The maximum strokes experienced by each landing-gear strut for the test vehicle landings are presented in table IV. The comparison of primary and secondary strut strokes between the test vehicle and the theoretical model are shown in figure 12. The stroke during each landing for each of the corresponding primary and secondary struts of the test vehicle and the theoretical model are plotted as abscissa and ordinate, respectively. The test data of table IV show that strut strokes were not as symmetric as they should be with symmetric 2-2 and 1-2-1 landings. This condition was particularly true for the secondary struts. Yaw oscillations experienced during launch of the test vehicle on the simulator combined with variations in pitch attitude, pitch motions, and surface conditions contributed to asymmetric stroking of the struts during the landing impact. These asymmetric results are considered to be realistic and representative of an actual landing; however, the theoretical approach assumes perfectly symmetric and planar landings and this assumption accounts for some of the scatter of the data in figure 12. In general, the agreement between experimental and theoretical results is good, and theoretical results are conservative in the case of large strokes.

Vehicle Center-of-Gravity Acceleration

The maximum center-of-gravity normal, longitudinal, and angular accelerations measured during the test-vehicle landings are presented in table V. The normal and angular accelerations experienced for the four general types of landings conducted are also shown in figure 13. The maximum normal acceleration experienced during landings of the test vehicle was approximately 2.2g, and the maximum angular acceleration was about 7.5 rad/s^2. The agreement of maximum normal and angular acceleration during each landing between the test vehicle and the theoretical model is shown in figure 14. Experimental and theoretical values for maximum normal acceleration (fig. 14(a)) are in good agreement whereas the data for angular acceleration (fig. 14(b)) show a larger amount of scatter. The greater difficulty in measuring angular accelerations together with the nonsymmetric landings contributed to greater scatter in the angular acceleration data than for the linear accelerations.

Vehicle Motions

The pitch-motion time histories obtained from motion pictures of five consecutive 1-2-1 landings are shown in figure 15 for vehicle launches which were intended to give the same touchdown pitch attitude and speed. Although the curves and table II indicate a substantial variation in these initial impact conditions, the pitch-motion trends of the vehicle were very similar during the 1-2-1 landing impacts, and the displacement along the time scale of individual time-history curves reflected the variation of initial impact conditions.

Landings at or near the same attitudes resulted in almost identical pitch time histories. The deviations in initial impact conditions were primarily caused by vehicle oscillations and inherent launch- and support-cable dynamics during launch and prior to initial impact.

The pitch-motion time histories for three 2-2 landings resulting in rocking motions are shown in figure 16. After initial impact on the rear legs, the vehicle rotates (pitches) downward to second impact on the front legs; then the rear legs lift off the surface ("rock up") and return to a third (final) impact. This sequence of events is illustrated by the sketches in figure 16. The solid lines are for the experimental landings, and the dashed lines are for theoretical landing simulations using the same touchdown conditions as for the experiment. Touchdown pitch attitude and vertical speed were to be held constant while horizontal speed was increased for each successive experimental landing. Vertical speed was almost constant for all three landings (see table II), and pitch attitude was essentially constant for landings 7 and 20; however, initial pitch attitude was low for landing 21. In addition, landing 7 was almost short (rear pads contacted partially on inclined ramp of elevated surface), and a negative pitch rate of about 0.031 rad/s was measured at initial contact for landing 21. Therefore, landing 20 was considered the best of the three landings since speed and attitude were stabilized.

During the three experimental landings (7, 20, and 21), the maximum rock-up attitude increased with increase in horizontal speed. The theoretical results do not show the same trend. The theoretical model appears relatively insensitive to the initial impact conditions at this point in the time history (1.0 to 2.0 seconds). However, landing 20 shows very good correlation between theory and experiment for pitch attitude trends, magnitude, and time. This agreement supports the ability of the theoretical analysis to predict vehicle motions and stability boundaries. More extensive correlation can be obtained with small and more controllable free-body dynamic models where uncertainties in initial impact conditions and support-cable dynamics can be minimized.

CONCLUDING REMARKS

Structural integrity of a prototype LM landing-gear system (struts and deployment trusses) was substantiated during 21 landings of a full-scale test vehicle at simulated lunar gravity and at earth ambient atmospheric conditions. Dynamic performance of the landing-gear struts was good for all landing conditions tested including those which produced near maximum shock-absorber strut strokes and loads. Theoretical results were

in agreement with experimental results obtained for landing accelerations, gear forces and strokes, and vehicle pitch motions.

Langley Research Center,
National Aeronautics and Space Administration,
Langley Station, Hampton, Va., January 9, 1969,
124-08-04-09-23.

APPENDIX A

CONVERSION OF U.S. CUSTOMARY UNITS TO SI UNITS

The International System of Units (SI) was adopted by the Eleventh General Conference on Weights and Measures held in Paris in 1960. (See ref. 2.) Conversion factors for the units used are given in the following table:

Physical quantity	U.S. Customary Unit	Conversion factor (*)	SI Unit (**)
Frequency	Cycles per second	1	hertz (Hz)
Length	$\begin{cases} \text{in.} \\ \text{ft} \end{cases}$	0.0254 0.3048	meters (m) meters (m)
Mass	slug	14.594	kilograms (kg)
Force	lbf	4.4482	newtons (N)
Moment of inertia . . .	slug-ft^2	1.3558	kilogram-meters^2 (kg-m^2)
Velocity	ft/sec	0.3048	meters/second (m/s)

*Multiply value given in U.S. Customary Unit by conversion factor to obtain equivalent value in SI Units.

**Prefixes to indicate multiples of units are as follows:

Prefix	Multiple
centi (c)	10^{-2}
kilo (k)	10^3

REFERENCES

1. Blanchard, Ulysse J.: Evaluation of a Full-Scale Lunar-Gravity Simulator by Comparison of Landing-Impact Tests of a Full-Scale and a 1/6-Scale Model. NASA TN D-4474, 1968.

2. Comm. on Metric Pract.: ASTM Metric Practice Guide. NBS Handbook 102, U.S. Dep. Com., Mar. 10, 1967.

TABLE I.- PERTINENT CHARACTERISTICS OF FULL-SCALE TEST VEHICLE
AND PROTOTYPE LANDING GEAR

Vehicle mass, slugs (kg) 441 (6440)

Moment of inertia, slug-ft^2 (kg-m^2)
Pitch 12 000 (16 300)
Yaw . . . . Constrained
Roll . . . . Constrained

Height of center of gravity above ground line, in. (m) 141 (3.58)

Landing-gear radius, in. (m) 167.5 (4.25)

Landing-gear mass, total, slugs (kg) 15.92 (232.3)
Primary-strut mass, each, slugs (kg) 2.72 (39.7)
Pad mass, slugs (kg) 0.75 (11.0)
Inner slide mass, slugs (kg) 0.93 (13.6)
Honeycomb cartridge mass, slugs (kg) 0.23 (3.4)
Primary-strut moment of inertia, each, slug-ft^2 (kg-m^2):
About axis normal to long strut axis:
Inner slide extended 28.4 (38.5)
Inner slide stroked 16.6 (22.5)
About long strut axis 0.6 (0.8)
Inner slide only with pad:
About axis normal to long axis 6.3 (8.5)
Secondary-strut mass, each, slugs (kg) 0.31 (4.5)
Honeycomb cartridge mass:
Tension 0.027 (0.39)
Compression 0.016 (0.23)
Deployment truss mass, each, slugs (kg) 0.64 (9.3)

Landing-gear strut stroke, in. (m):
Primary, first stage 10.0 (0.254)
Primary, second stage 23.0 (0.584)
Secondary, compression 9.8 (0.249)
Secondary tension, first stage 4.0 (0.102)
Secondary tension, second stage 13.0 (0.330)

Honeycomb-cartridge static crush force (±5%), lbf (kN):
Primary, first stage 4090 (18.2)
Primary, second stage 8640 (38.4)
Secondary compression 4090 (18.2)
Secondary tension, first stage 460 (2.0)
Secondary tension, second stage 4550 (20.2)

Honeycomb-cartridge design dynamic crush force, lbf (kN):
Primary, first stage 4500 (20.0)
Primary, second stage 9500 (42.3)
Secondary compression 4500 (20.0)
Secondary tension, first stage 500 (2.2)
Secondary tension, second stage 5000 (22.2)

TABLE II.- INITIAL CONDITIONS FOR LANDING-IMPACT TESTS OF FULL-SCALE VEHICLE

Landing number	Gear orientation	Pitch attitude, deg	V_v, ft/sec (m/s)	V_h, ft/sec (m/s)	Cartridge average static crush force, lbf (kN)					Pad-surface friction coefficient	Surface characteristic
					Primary struts		Secondary struts				
					C_1	C_2	C	T_1	T_2		
1	2-2	0	10.0 (3.0)	0 (0)	4095 (18.2)	8815 (39.2)	4135 (18.4)	445 (1.98)	4545 (20.2)	0.4	Flat
2	2-2	$8\frac{2}{3}$	10.0 (3.0)	0 (0)	4260 (18.9)	8795 (39.1)	4135 (18.4)	455 (2.02)	4545 (20.2)	0.4	Flat
3	2-2	8	10.0 (3.0)	4.5 (1.4)	4115 (18.3)	8750 (38.9)	4245 (18.9)	455 (2.02)	4560 (20.3)	0.4	Flat
4	2-2	$7\frac{1}{4}$	10.0 (3.0)	5.0 (1.5)	4115 (18.3)	8815 (39.2)	4135 (18.4)	445 (1.98)	4585 (20.4)	∞	Flat
5	2-2	9	10.0 (3.0)	5.5 (1.7)	4140 (18.4)	8855 (39.4)	4090 (18.2)	450 (2.00)	4545 (20.2)	∞	Flat
6	2-2	$9\frac{3}{4}$	10.0 (3.0)	0 (0)	4195 (18.7)	8775 (39.0)	4110 (18.3)	445 (1.98)	4465 (19.9)	∞	Elevation at gears 1 and 4
7	2-2	8	10.0 (3.0)	5.0 (1.5)	4080 (18.1)	8780 (39.1)	4100 (18.2)	450 (2.00)	4500 (20.0)	∞	Elevation at gears 1 and 4
8	1-2-1	$8\frac{1}{2}$	7.5 (2.3)	5.0 (1.5)	4205 (18.7)	8895 (39.6)	4080 (18.1)	445 (1.98)	4565 (20.3)	∞	Elevation at gear 4
9	1-2-1	$6\frac{1}{4}$	8.0 (2.4)	7.0 (2.1)	4255 (18.9)	8605 (38.3)	4040 (18.0)	450 (2.00)	4525 (20.1)	∞	Flat
10	1-2-1	7	8.5 (2.6)	6.0 (1.8)	4255 (18.9)	8780 (39.1)	4065 (18.1)	455 (2.02)	4575 (20.3)	∞	Elevation at gear 4
11	1-2-1	$7\frac{2}{3}$	7.5 (2.3)	4.5 (1.4)	4225 (18.8)	8605 (38.3)	4070 (18.1)	450 (2.00)	4575 (20.3)	∞	Elevation at gear 4
12	1-2-1	8	7.0 (2.1)	5.0 (1.5)	4230 (18.8)	8670 (38.6)	4085 (18.2)	455 (2.02)	4555 (20.3)	∞	Elevation at gear 4
13	1-2-1	$9\frac{1}{2}$	7.0 (2.1)	5.0 (1.5)	4205 (18.7)	8725 (38.8)	4115 (18.3)	445 (1.98)	4545 (20.2)	∞	Elevation at gear 4
14	1-2-1	$9\frac{3}{4}$	7.0 (2.1)	5.0 (1.5)	4180 (18.6)	8745 (38.9)	4085 (18.2)	450 (2.00)	4515 (20.1)	∞	Elevation at gear 4
15	1-2-1	$9\frac{1}{4}$	7.0 (2.1)	3.5 (1.1)	4120 (18.3)	8640 (38.4)	4080 (18.1)	445 (1.98)	4545 (20.2)	∞	Elevation at gear 4
16	1-2-1	$\frac{1}{2}$	14.0 (4.3)	0 (0)	4170 (18.5)	8815 (39.2)	4040 (18.0)	450 (2.00)	4630 (20.6)	0.4	Elevation at gears 2 and 4
17	1-2-1	$-\frac{1}{4}$	9.0 (2.7)	0 (0)	4185 (18.6)	8650 (38.5)	4040 (18.0)	450 (2.00)	4590 (20.4)	0.15	Elevation at gears 2 and 4
18	2-2	$-5\frac{1}{4}$	9.5 (2.9)	5.0 (1.5)	4155 (18.5)	8740 (38.9)	4040 (18.0)	455 (2.02)	4550 (20.2)	∞	Flat
19	2-2	-4	10.0 (3.0)	5.0 (1.5)	4170 (18.5)	8690 (38.7)	4050 (18.0)	450 (2.00)	4610 (20.5)	∞	Flat
20	2-2	$7\frac{1}{2}$	9.5 (2.9)	5.5 (1.7)	4185 (18.6)	8650 (38.5)	4095 (18.2)	445 (1.98)	4630 (20.6)	∞	Elevation at gears 1 and 4
21	2-2	$5\frac{2}{3}$	10.0 (3.0)	6.5 (2.0)	4095 (18.2)	8830 (39.3)	4035 (17.9)	450 (2.00)	4460 (19.8)	∞	Elevation at gears 1 and 4

15

TABLE III.- LANDING GEAR EXPERIMENTAL FORCE DATA

[NR denotes no data recorded; blank spaces indicate no honeycomb crush.]

(a) U.S. Customary Units

Strut stroking force, lbf

Landing number	Landing gear 1								Landing gear 2							
	Primary strut		Secondary strut						Primary strut		Secondary strut					
			Left			Right					Left			Right		
	C_1	C_2	C	T_1	T_2	C	T_1	T_2	C_1	C_2	C	T_1	T_2	C	T_1	T_2
1	4866	9 384		646			540		4830	9 660		NR			663	
2	5213			729			506		6030			NR	NR		707	
3	NR			NR			604	4737	5309	9 412		611			707	
4	4657			601			574	5118	5309	9 894	4880	611			707	
5	4726			684		4267	595	5115	5335	9 040	4240	NR			659	
6	4657	10 320		684		4191	NR		6064		4494	520			710	
7	4500			684			620	4957	5469	9 274	4794	694			659	
8	6287		4429				687		5469	9 988		650			659	
9	NR	NR	NR	NR			NR	NR	NR	NR	NR	NR			NR	
10	6340		4000	430			NR		5588	9 393		482			660	
11	6403		4558				620		5960	9 300		482			666	
12	6940		4171	556			566		5232	9 512		482			703	
13	6740		4532				715		5404	9 967		520			703	
14	6916		4300	599			674		5120	9 988		569			747	
15	7150		4257				NR		5113	9 870		477		4960	791	
16	5288			575					6531	12 459		558	4890		891	5168
17									5564			600	4975		779	5060
18	5769			644			627		6411	11 007	4438				692	
19	6195			715			615		6290	11 128	4608	600			648	
20	5117			637			579	5018	5564	9 919	4566	729			735	
21	5168			680			675	4921	5201	10 160	4523	858			692	

Landing number	Landing gear 3								Landing gear 4							
	Primary strut		Secondary strut						Primary strut		Secondary strut					
			Left			Right					Left			Right		
	C_1	C_2	C	T_1	T_2	C	T_1	T_2	C_1	C_2	C	T_1	T_2	C	T_1	T_2
1	4802	9 484		441			522		4700	9 659		507			400	
2	5677			471			565		5100	10 300		669			444	
3	5349	10 222		557			609		NR			585	5380		444	
4	5230	9 390		470		4980	565		NR			586	5104		444	
5	5432	9 658		473		4250	620	4900	NR			582	4950		448	
6	5397			473		4378	555		NR	NR	4609	541			448	
7	5140	9 160		474		4760	733		NR			582	4826		448	
8	NR			523		4718	647		5221			624			448	
9	NR		NR	NR		NR	NR		NR			NR			NR	
10	NR			523		4420	510		4767			666			493	
11	NR			479		4590	604		5560			672			498	
12	NR			479		NR	NR		4880			707			498	4887
13	NR			523		NR	NR		4767			624			498	
14	NR			566		NR	NR		4881			666			543	
15	NR			479		4378	431		4540			666			498	
16	5090			445			528		NR	NR		771	5400		543	5199
17				480			475		6278			672	5168		582	5103
18	6181	10 908		490		4888	573		4773			546			497	
19	6120	11 040		475		4711	470		5883			588			492	
20	5696	10 060		480		4845	604		4995			546	5480		448	
21	5696	10 059		490		4412	704		4981			630	4916		493	

TABLE III.- LANDING GEAR EXPERIMENTAL FORCE DATA – Concluded

(b) SI Units

Strut stroking force, Newtons (kN)

Landing number	Landing gear 1								Landing gear 2							
	Primary strut		Secondary strut						Primary strut		Secondary strut					
			Left			Right					Left			Right		
	C_1	C_2	C	T_1	T_2	C	T_1	T_2	C_1	C_2	C	T_1	T_2	C	T_1	T_2
1	21.6	41.7		2.87			2.40		21.5	43.0		NR			2.95	
2	23.2			3.24			2.25		26.8			NR	NR		3.14	
3	NR			NR			2.69	21.1	23.6	41.9		2.72			3.14	
4	20.7			2.67			2.55	22.8	23.6	44.0	21.7	2.72			3.14	
5	21.0			3.04		19.0	2.65	22.9	23.7	40.2	18.9	NR			2.93	
6	20.7	45.9		3.04		18.6	NR		27.0		20.0	2.31			3.16	
7	20.0			3.04			2.76	22.0	24.3	41.2	21.3	3.09			2.93	
8	28.0		19.7				3.06		24.3	44.4		2.89			2.93	
9	NR		NR	NR			NR	NR	NR	NR	NR	NR			NR	
10	28.2		17.8	1.91			NR		24.9	41.8		2.14			2.94	
11	28.5		20.3				2.76		26.5	41.4		2.14			2.96	
12	30.9		18.6	2.47			2.52		23.3	42.3		2.14			3.13	
13	30.0		20.2				3.18		24.0	44.3		2.31			3.13	
14	30.8		19.1	2.66			3.00		22.8	44.4		2.53			3.32	
15	31.8		18.9				NR		22.7	43.9		2.12		22.1	3.52	
16	23.5			2.56					29.0	55.4		2.48	21.7		3.96	23.0
17									24.7			2.67	22.1		3.46	22.5
18	25.7			2.86			2.79		28.5	49.0	19.7				3.08	
19	27.6			3.18			2.74		28.0	49.5	20.5	2.67			2.88	
20	22.8			2.83			2.58	22.3	24.7	44.1	20.3	3.24			3.27	
21	23.0			3.03			3.00	21.9	23.1	45.2	20.1	3.82			3.08	

Landing number	Landing gear 3								Landing gear 4							
	Primary strut		Secondary strut						Primary strut		Secondary strut					
			Left			Right					Left			Right		
	C_1	C_2	C	T_1	T_2	C	T_1	T_2	C_1	C_2	C	T_1	T_2	C	T_1	T_2
1	21.4	42.2		1.96			2.32		20.9	43.0		2.25			1.78	
2	25.2			2.09			2.51		22.7	45.8		2.98	23.9		1.97	
3	23.8	45.5		2.48			2.71		NR			2.60	23.9		1.97	
4	23.3	41.8		2.09		22.1	2.51		NR			2.61	22.7		1.97	
5	24.2	43.0		2.10		18.9	2.76	21.8	NR			2.59	22.0		1.99	
6	24.0			2.10		19.5	2.47		NR	NR	20.5	2.41			1.99	
7	22.9	40.7		2.11		21.2	3.26		NR			2.59	21.5		1.99	
8	NR			2.33		21.0	2.88		23.2			2.78			1.99	
9	NR		NR	NR	NR	NR	NR		NR			NR			NR	
10	NR			2.33		19.7	2.27		21.2			2.96			2.19	
11	NR			2.13		20.4	2.69		24.7			2.99			2.21	
12	NR			2.13		NR	NR		21.7			3.14			2.21	21.7
13	NR			2.33		NR	NR		21.2			2.78			2.21	20.7
14	NR			2.52		NR	NR		21.7			2.96			2.41	22.1
15	NR			2.13		19.5	1.92		20.2			2.96	21.6		2.21	
16	22.6			1.98			2.35		NR	NR		3.43	24.0		2.41	23.1
17				2.13			2.11		27.9			2.99	23.0		2.59	22.7
18	27.5	48.5		2.18		21.7	2.55		21.2			2.43			2.21	
19	27.2	49.1		2.11		21.0	2.09		26.2			2.62			2.19	
20	25.3	44.7		2.13		21.6	2.69		22.2			2.43	24.4		1.99	
21	25.3	44.7		2.18		19.6	3.13		22.2			2.80	21.9		2.19	

17

TABLE IV.- LANDING GEAR EXPERIMENTAL STROKE DATA

(a) U.S. Customary Units

Strut maximum stroke, in.

Landing number	Landing gear 1 Primary strut	Secondary strut Left C	Left T	Right C	Right T	Landing gear 2 Primary strut	Secondary strut Left C	Left T	Right C	Right T
1	11.7		2.2		3.3	11.2		2.8		3.1
2	9.9		4.0		3.9	9.1		4.8		2.6
3	9.2		2.8		4.8	14.5		3.7		3.9
4	9.6		.7		4.8	13.9		3.9		3.9
5	9.5		.3	0.2	5.5	12.0	1.6	4.0		3.2
6	11.9		2.7	5.5	.8	7.5	1.2	.4		2.4
7	9.6		.6		4.9	15.4	2.8	2.6		3.9
8	2.1	1.2			4.0	21.8		2.5		1.6
9	9.9	.8	1.6		5.3	18.7	1.0	3.9		1.7
10	4.9	.4	1.9		3.9	28.2		3.9		3.9
11	3.3	.8			4.0	21.8		3.9		3.6
12	2.2	.8	1.1		3.9	23.8		2.9		1.5
13	3.0	.5			3.9	23.4		2.7		1.3
14	2.9	.6	.1		2.7	23.9		2.3		1.2
15	2.1	1.5			2.6	21.0		1.7	1.8	1.1
16	3.2		1.1			18.0		9.8		9.2
17						.2		13.2		12.6
18	.5		.8		1.7	12.9	9.0			4.0
19	1.0		1.5		4.0	14.0	7.9	4.0		4.0
20	8.9		.2		4.9	14.9	4.5	2.2		3.9
21	6.8		.4		5.9	16.4	3.0	2.4		4.0

Landing number	Landing gear 3 Primary strut	Secondary strut Left C	Left T	Right C	Right T	Landing gear 4 Primary strut	Secondary strut Left C	Left T	Right C	Right T
1	11.2		3.1		1.7	11.3		3.5		3.5
2	9.4		3.9		4.0	10.3		3.8		4.0
3	14.9		4.0		4.0	9.9		4.8		3.9
4	16.7		3.9	0.3	3.9	7.4		5.7		3.9
5	14.3		4.0	2.3	4.1	9.4		7.4		4.0
6	9.0		2.2	.9	1.2	11.8	2.4	1.2		3.9
7	15.8		3.9	4.1	3.2	8.3		4.1		3.9
8	2.2		4.0	1.7	1.8	5.0		3.9		4.0
9	9.8		5.1	.8	3.9	3.6		3.9		4.0
10	4.4		3.9	2.9	2.1	4.6		3.9		3.9
11	1.2		4.0	2.3	.3	4.7		4.0		4.0
12	2.6		4.0	1.5	1.8	4.1		3.7		4.3
13	1.7		3.9	1.2	1.0	4.9		3.2		3.6
14	1.3		2.4	1.2	1.1	4.6		2.8		3.2
15	.6		2.5	1.5	.6	5.7		2.7		3.3
16	4.5		.4		1.2	18.0		7.7		7.7
17			.6		1.4			13.3		15.4
18	14.3		4.0	5.4	1.5	.2		4.0		4.0
19	14.4		4.0	4.0	4.0	.4		4.0		4.0
20	15.8		3.9	4.7	2.3	7.0		4.2		3.7
21	17.9		4.0	3.0	2.2	7.2		5.6		3.1

18

TABLE IV.- LANDING GEAR EXPERIMENTAL STROKE DATA – Concluded

(b) SI Units

Landing number	Strut maximum stroke, meters									
	Landing gear 1					Landing gear 2				
	Primary strut	Secondary strut				Primary strut	Secondary strut			
		Left		Right			Left		Right	
		C	T	C	T		C	T	C	T
1	0.297		0.056		0.084	0.284		0.071		0.079
2	.251		.102		.099	.231		.122		.066
3	.234		.071		.122	.368		.094		.099
4	.244		.018		.122	.353		.099		.099
5	.241		.008	0.005	.140	.305	0.041	.102		.081
6	.302		.069	.140	.020	.191	.030	.010		.061
7	.244		.015		.124	.391	.071	.066		.099
8	.053	0.030			.102	.554		.064		.041
9	.251	.020	.041		.135	.475	.025	.099		.043
10	.124	.010	.048		.099	.716		.099		.099
11	.084	.020			.102	.554		.099		.091
12	.056	.020	.028		.099	.605		.074		.038
13	.076	.013			.099	.594		.069		.033
14	.074	.015	.003		.069	.607		.058		.033
15	.053	.038			.066	.533		.043	0.046	.028
16	.081		.028			.457		.249		.234
17						.005		.335		.320
18	.013		.020		.043	.328	.229			.102
19	.025		.038		.102	.356	.201	.102		.102
20	.226		.005		.124	.378	.114	.056		.099
21	.173		.010		.150	.417	.076	.061		.102
	Landing gear 3					Landing gear 4				
1	0.284		0.078		0.043	0.287		0.089		0.089
2	.239		.099		.102	.262		.097		.102
3	.378		.102		.102	.251		.122		.099
4	.424		.099	0.008	.099	.188		.145		.099
5	.363		.102	.058	.104	.239		.188		.102
6	.229		.056	.023	.030	.300	0.061	.030		.099
7	.401		.099	.102	.081	.211		.104		.099
8	.056		.102	.043	.046	.127		.099		.102
9	.249		.130	.020	.099	.091		.099		.102
10	.112		.099	.074	.053	.117		.099		.099
11	.030		.102	.058	.008	.119		.102		.102
12	.066		.102	.038	.046	.104		.094		.109
13	.043		.099	.030	.025	.124		.081		.091
14	.033		.061	.030	.028	.117		.071		.081
15	.015		.064	.038	.015	.145		.069		.084
16	.114		.010		.030	.457		.196		.196
17			.015		.036			.338		.391
18	.363		.102	.137	.038	.005		.102		.102
19	.366		.102	.127	.102	.010		.102		.102
20	.401		.099	.119	.058	.178		.107		.094
21	.455		.102	.076	.056	.183		.142		.079

TABLE V.- TEST VEHICLE EXPERIMENTAL ACCELERATION DATA

| Landing number | Maximum acceleration | | | | |
| | Normal, g units | Longitudinal, g units | | Angular, rad/s^2 | |
		Positive	Negative	Positive	Negative
1	2.2	0.00	0.00	1.69	1.97
2	1.8	.45	.29	5.29	2.65
3	2.0	.27	.70	6.67	3.20
4	1.3	.21	1.12	5.85	6.27
5	1.5	.24	1.12	7.31	4.35
6	1.2	.83	.67	2.79	2.23
7	1.1	.19	1.01	5.10	6.48
8	1.6	.13	.82	4.55	2.21
9	1.6	.13	1.03	3.86	2.07
10	1.3	.16	.73	4.27	2.07
11	1.6	.11	.80	4.69	4.14
12	1.6	.13	.75	3.90	2.51
13	1.7	.14	.91	3.72	4.00
14	1.7	.13	1.08	4.88	4.88
15	1.7	.13	1.00	5.85	5.29
16	2.3	.00	.00	.00	.00
17	1.0	.19	.16	1.25	1.11
18	1.3	.00	.79	2.37	4.18
19	1.7	.00	.85	2.67	6.86
20	1.3	.21	1.08	5.15	3.20
21	1.4	.21	1.32	5.43	3.20
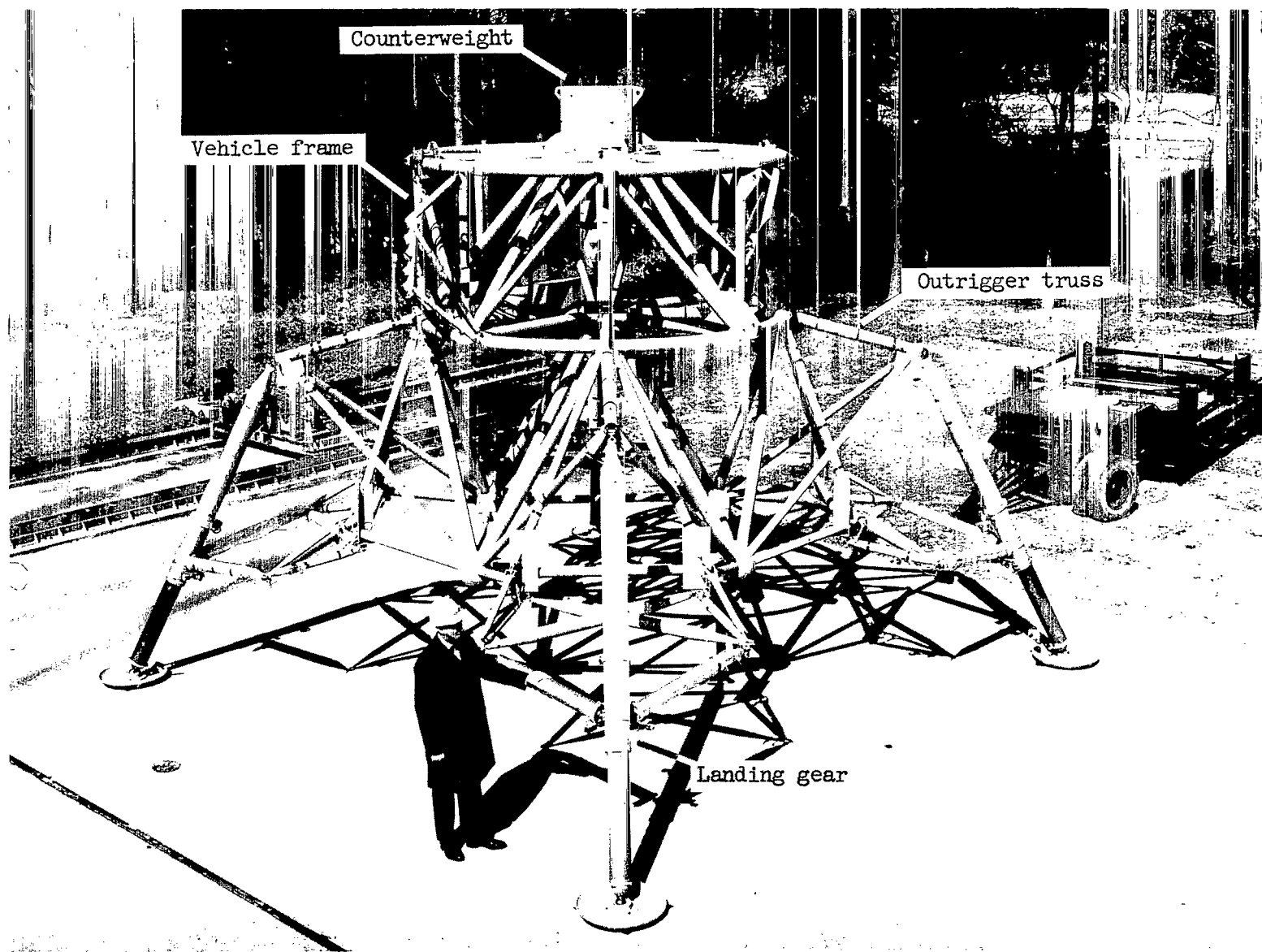
Figure 1.- Photograph of full-scale test vehicle.

L-68-2029.1
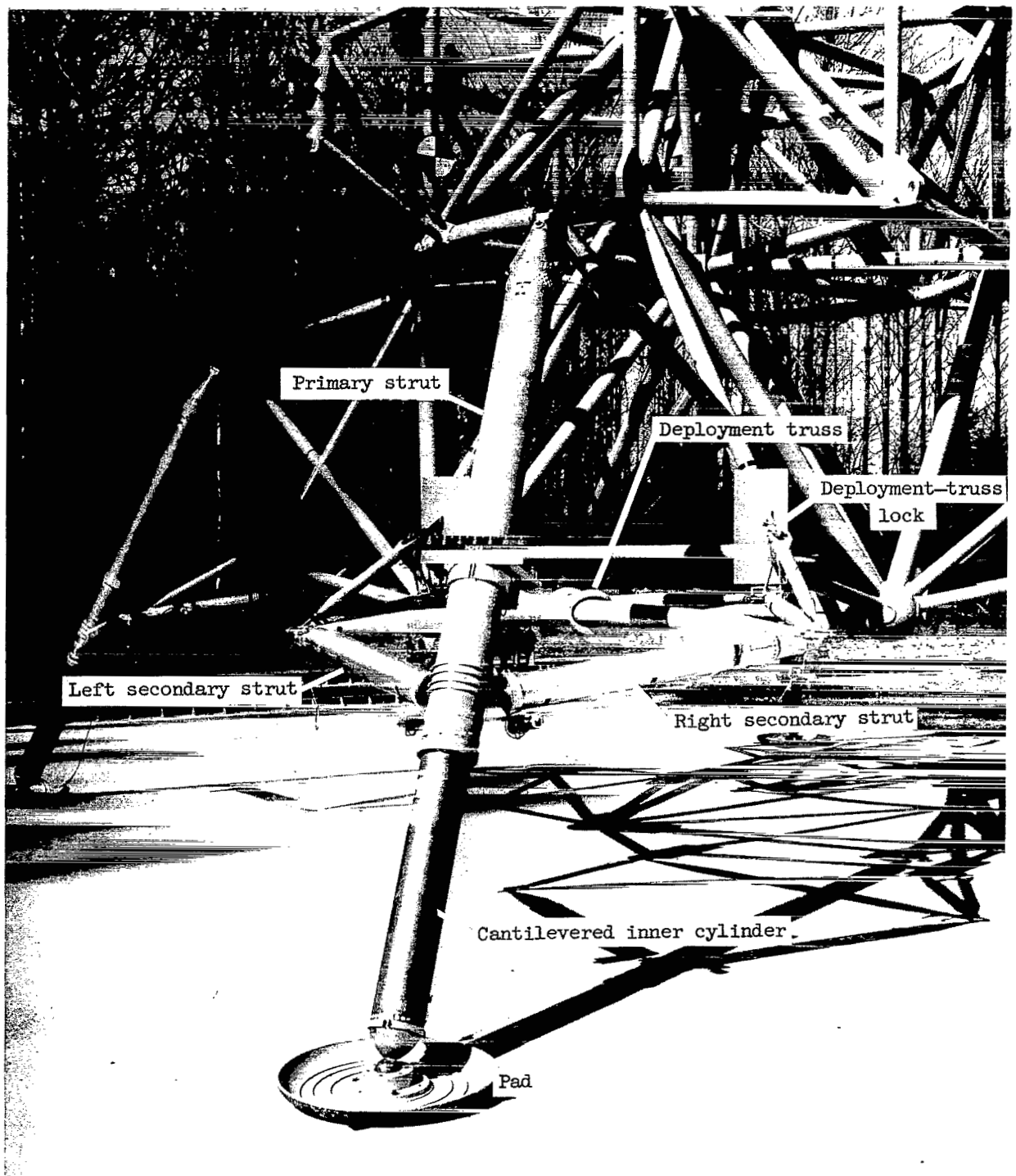
Figure 2.- Photograph of prototype landing gear.

L-68-2028.1

Outer cylinder

Bearing

Bearing

Inner cylinder

Crushable aluminum honeycomb cartridge

```
 0   2   4   6   8   10  12
           INCHES
 0      10      20      30
        CENTIMETERS
```
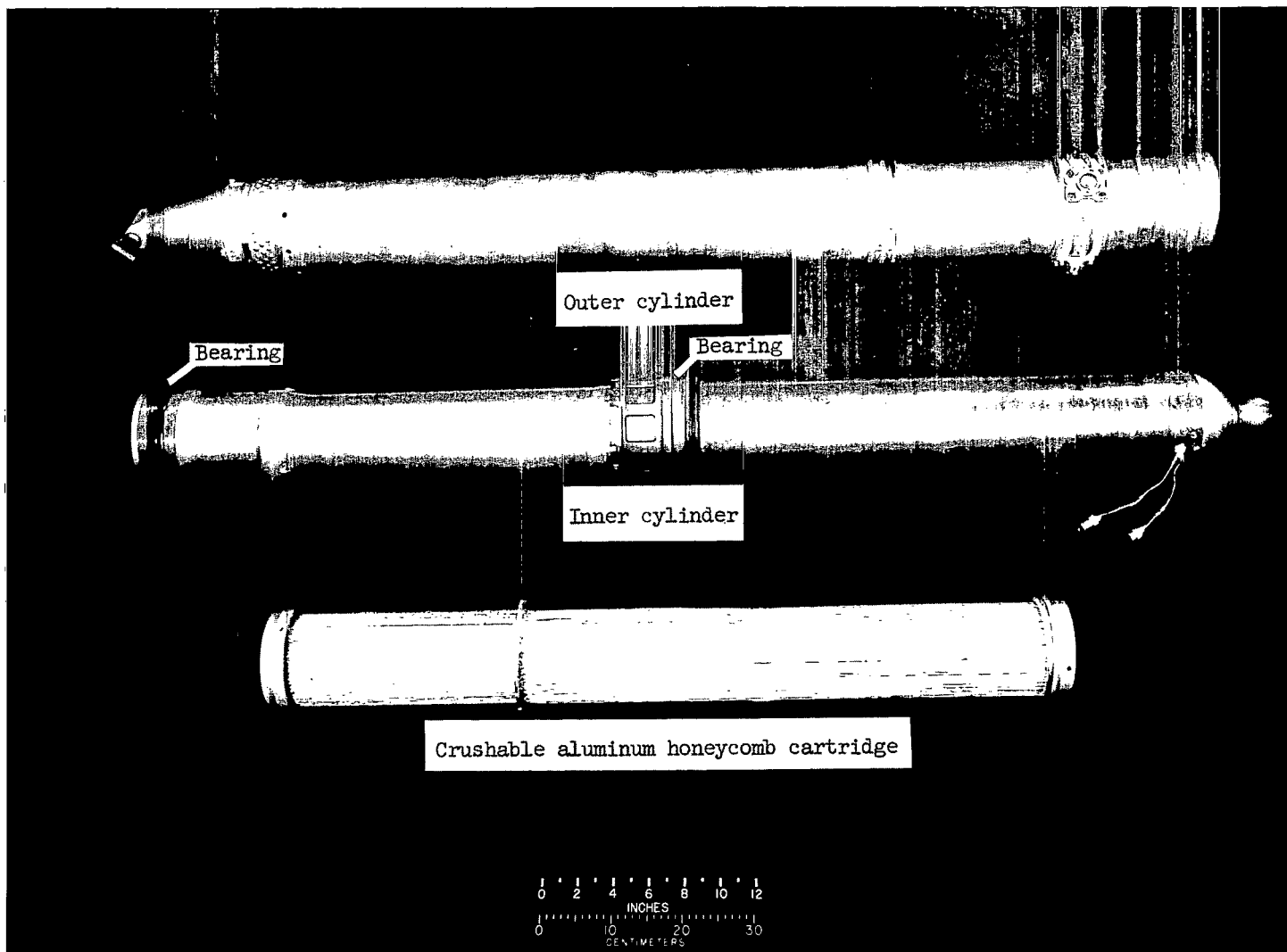
(a) Primary strut.

Figure 3.- Photographs of landing-gear shock-absorber strut components.

L-68-1247.1

Inner cylinder

Outer cylinder

Double-acting stroke linkage

Tension-stroke cartridge

Compression-stroke cartridge

Crushable aluminum honeycomb cartridges

INCHES

CENTIMETERS
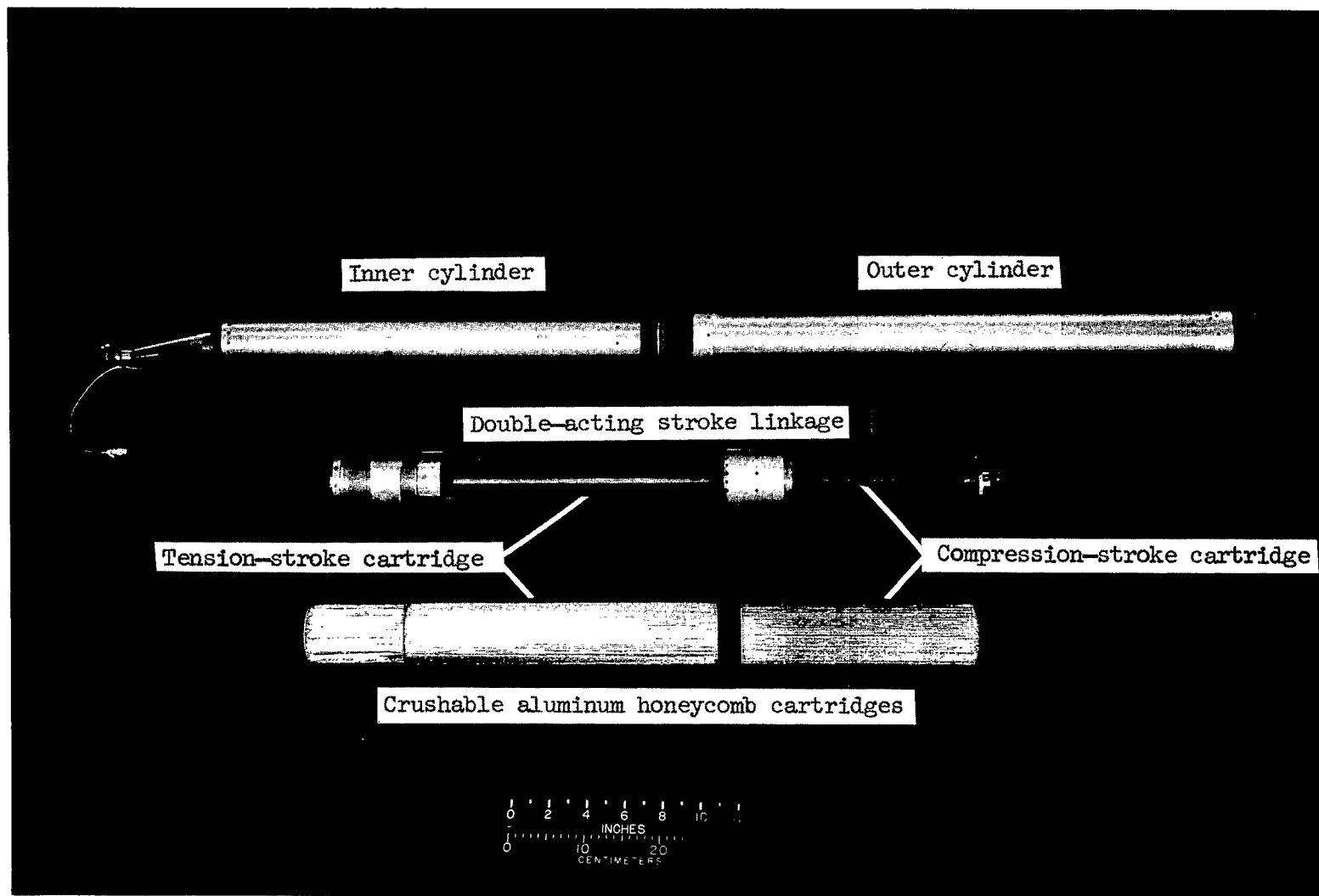
(b) Secondary strut.

Figure 3.- Concluded.

L-68-1249.1

Gear-down lock

Vehicle outrigger-truss pivot

Secondary-strut pivot

INCHES
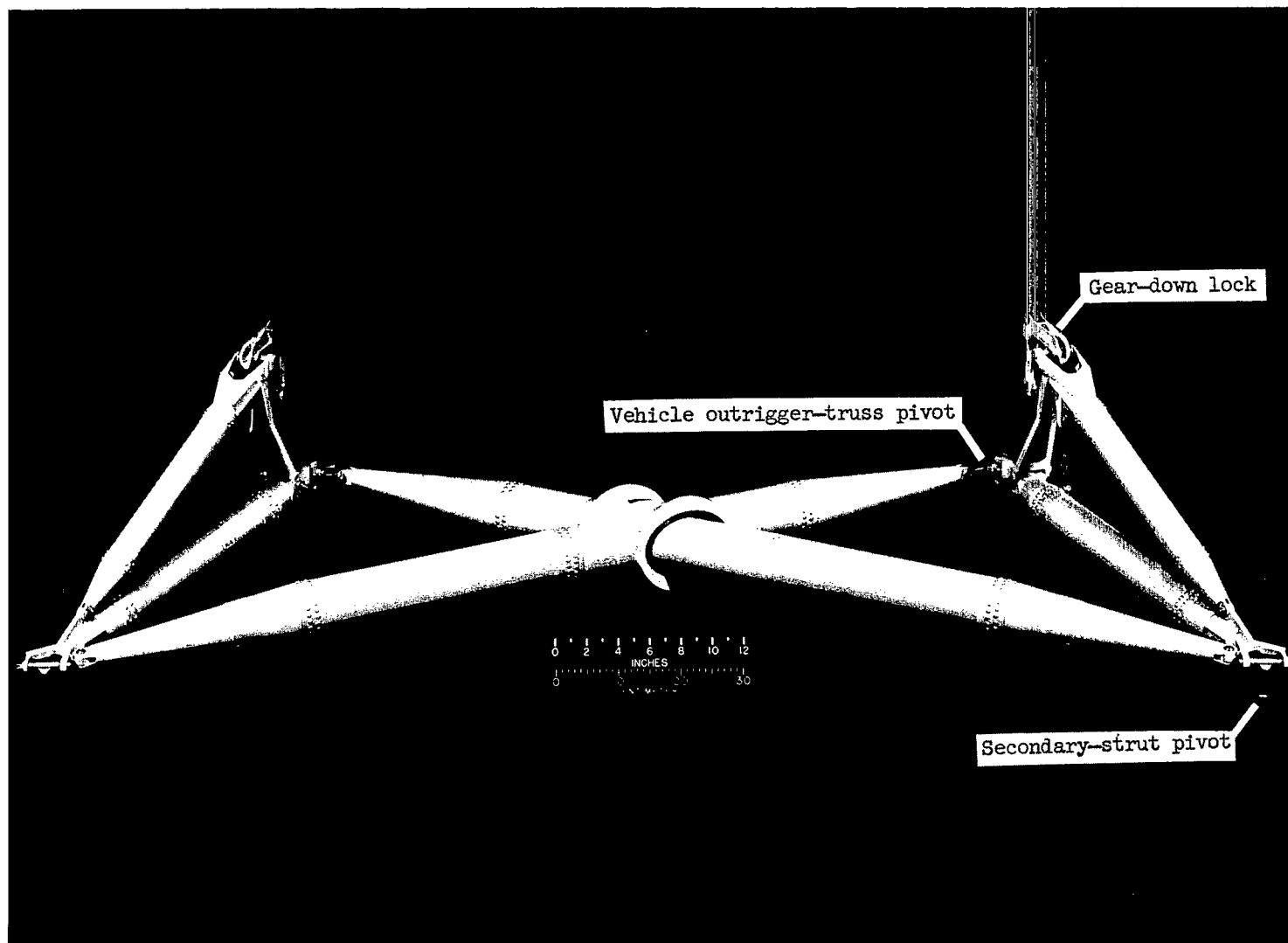
Figure 4.- Photograph of landing-gear deployment truss.

L-68-1743.1
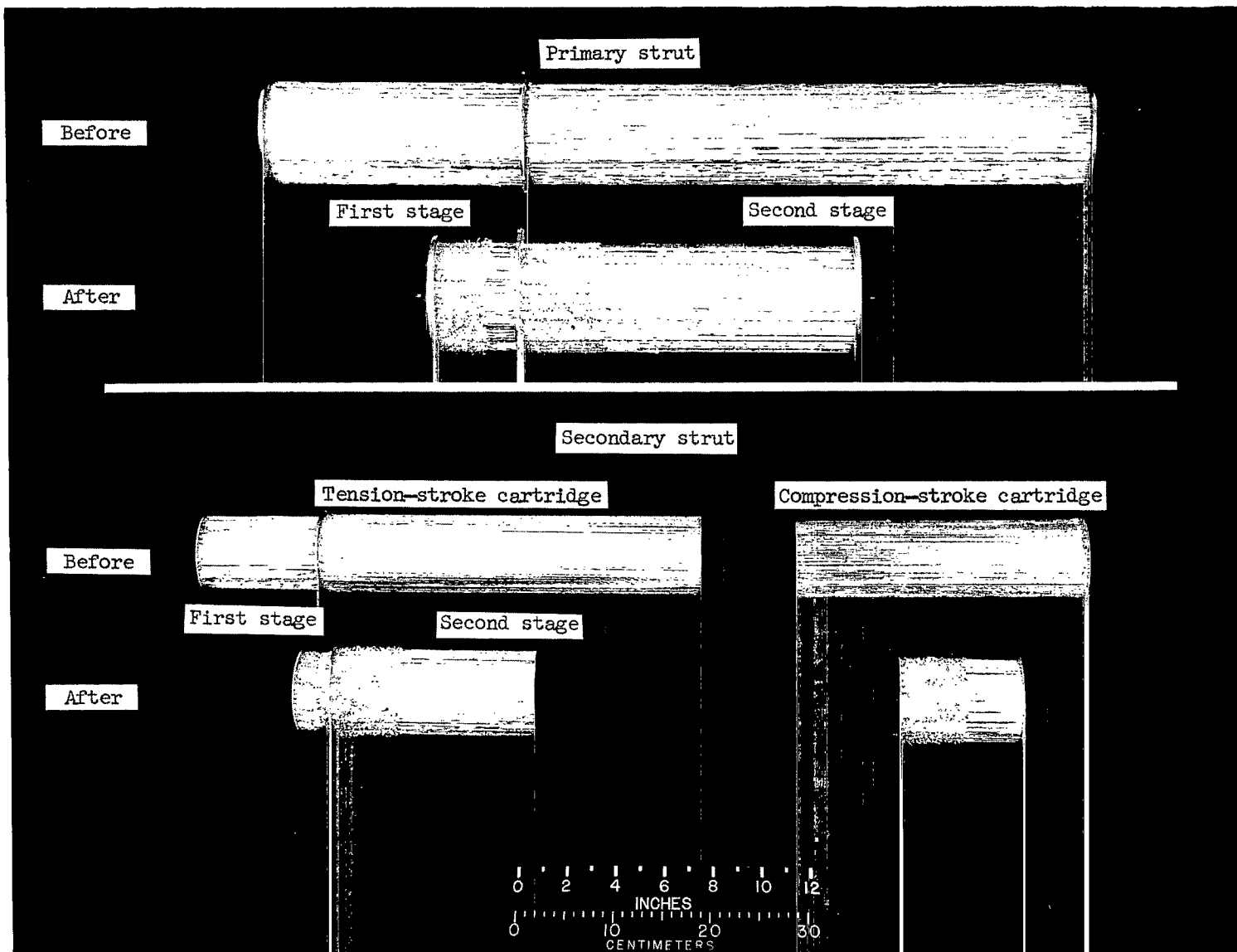
Figure 5.- Photograph of aluminum honeycomb shock-absorbing cartridges from landing-gear struts before and after impact crush.   L-68-1250.1

Release—cable winch

Instrumentation and service trailer

Lunar landing research facility structure

Test vehicle

Landing—surface

Release—cable winches

Photographic grid
(6 × 6—foot squares (1.8 × 1.8 m))
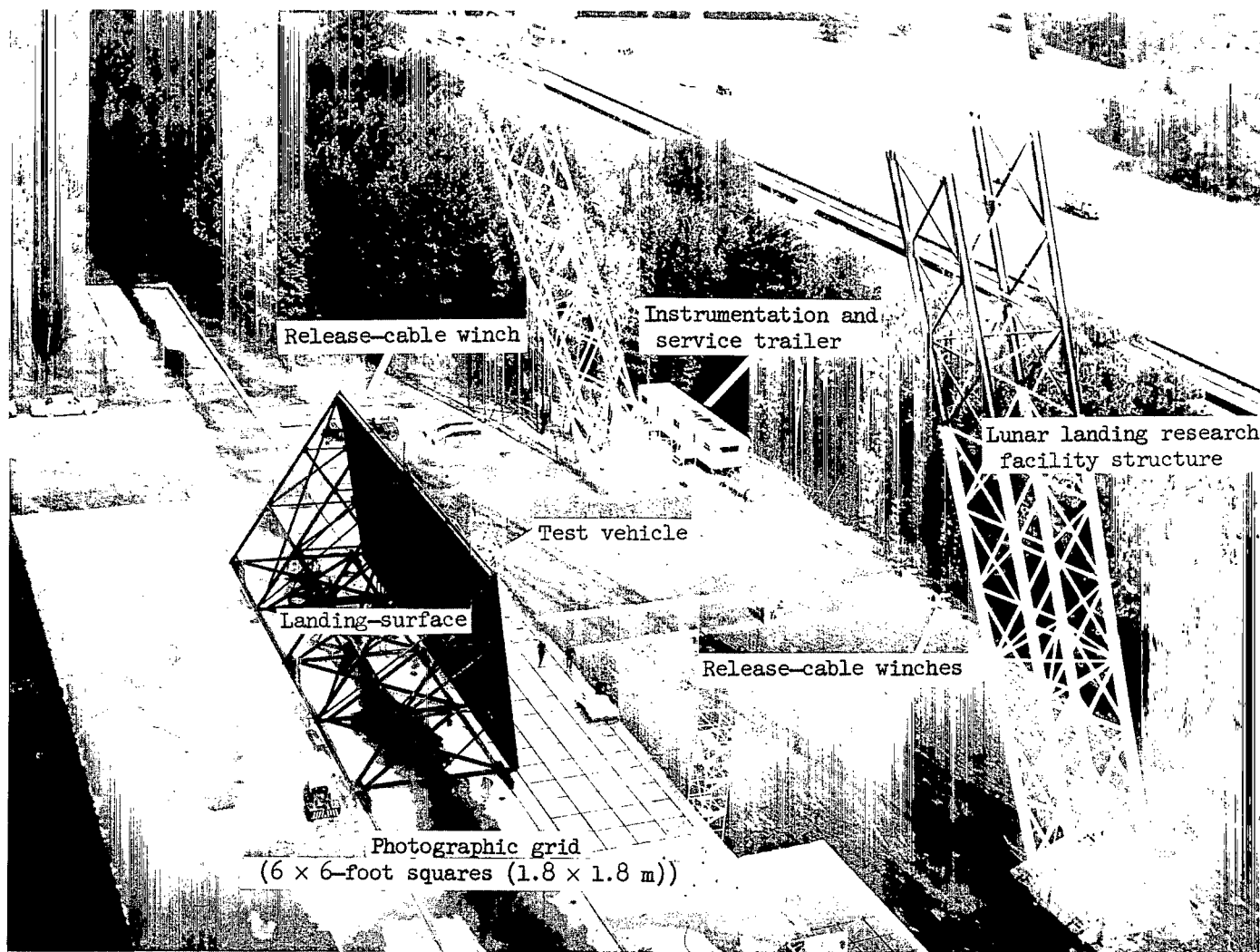
(a) Overhead view.

Figure 6.- Photographs of full-scale lunar-gravity impact simulator.

L-67-5995.1

27

Overhead trolley and track

Support cable

Release cables

Landing surface

Full-scale test vehicle

Instrument cable
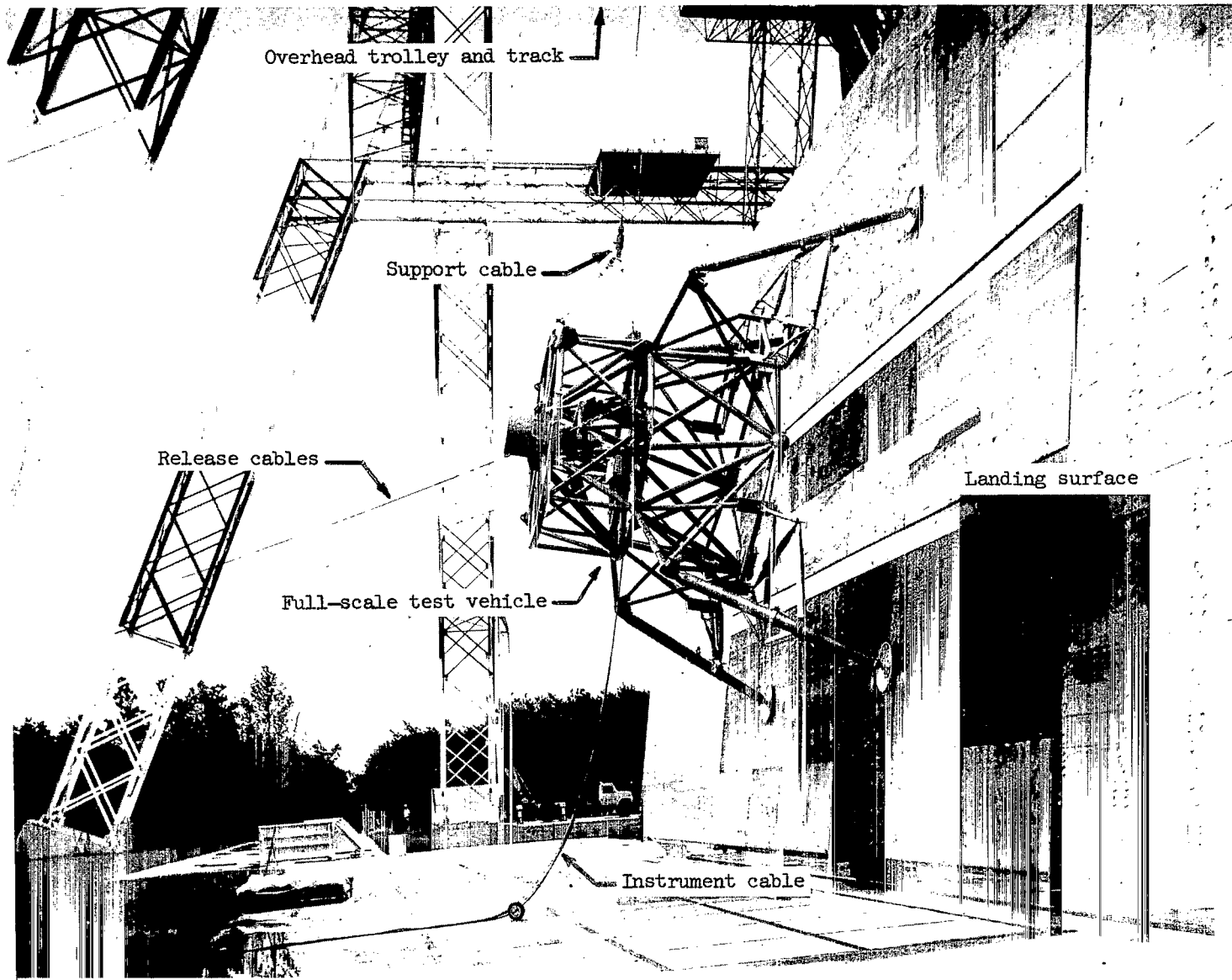
(b) Ground view.

Figure 6.- Concluded.

L-67-5997.1
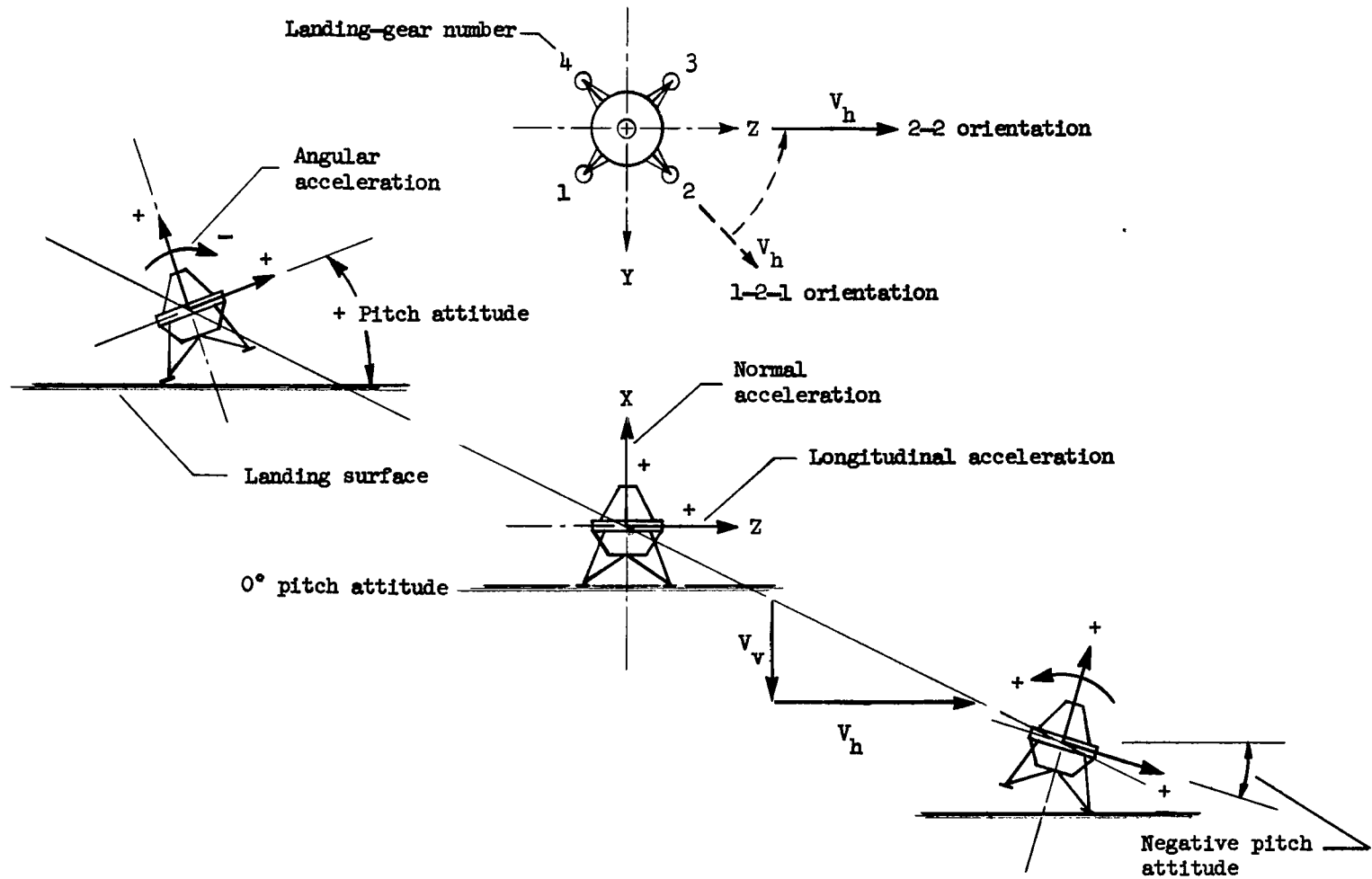
Figure 7.- Sketches identifying axes, accelerations, attitudes, velocities, and flight path.
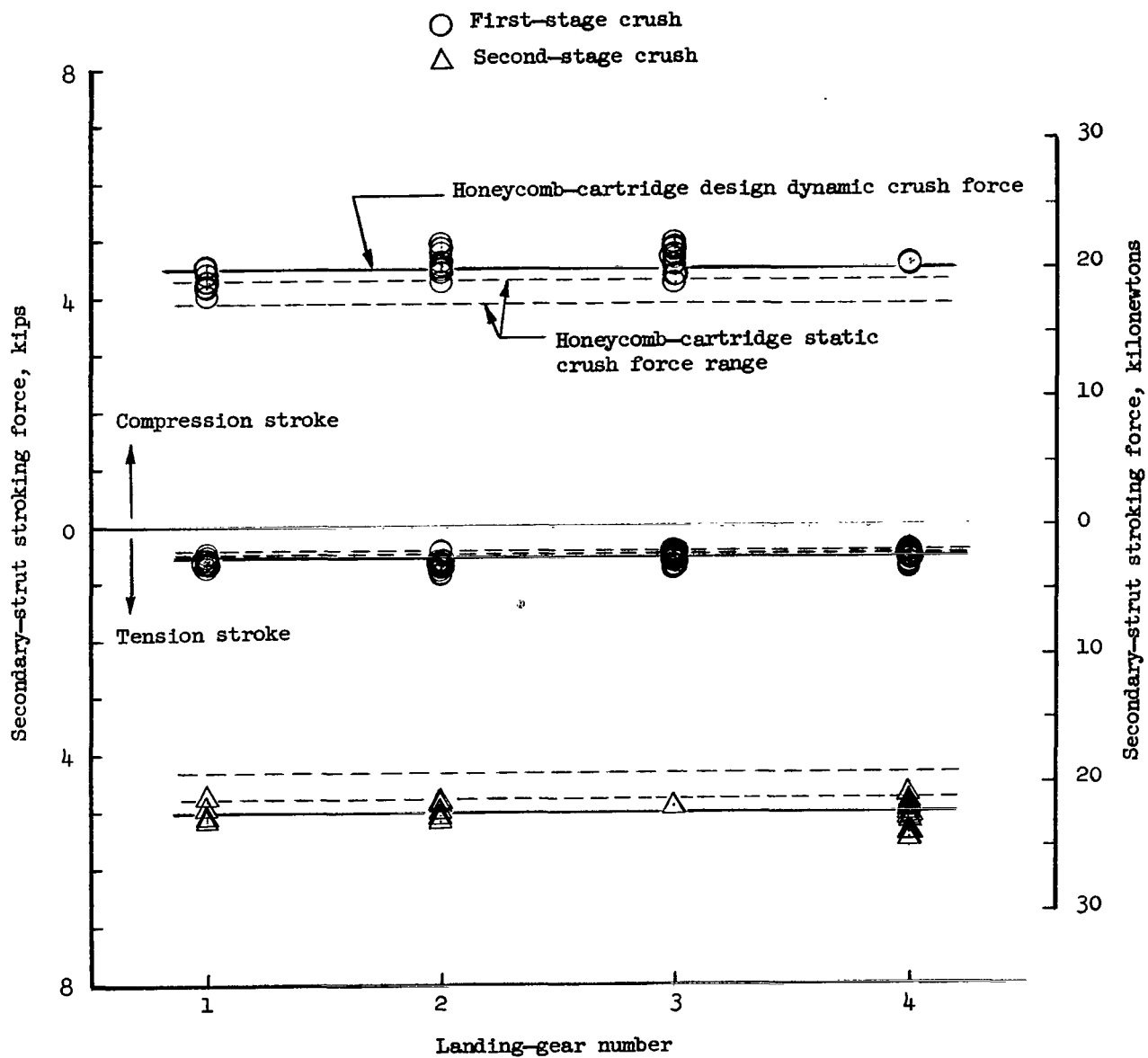
Figure 8.- Stroking forces measured on landing-gear secondary struts during test vehicle landings.
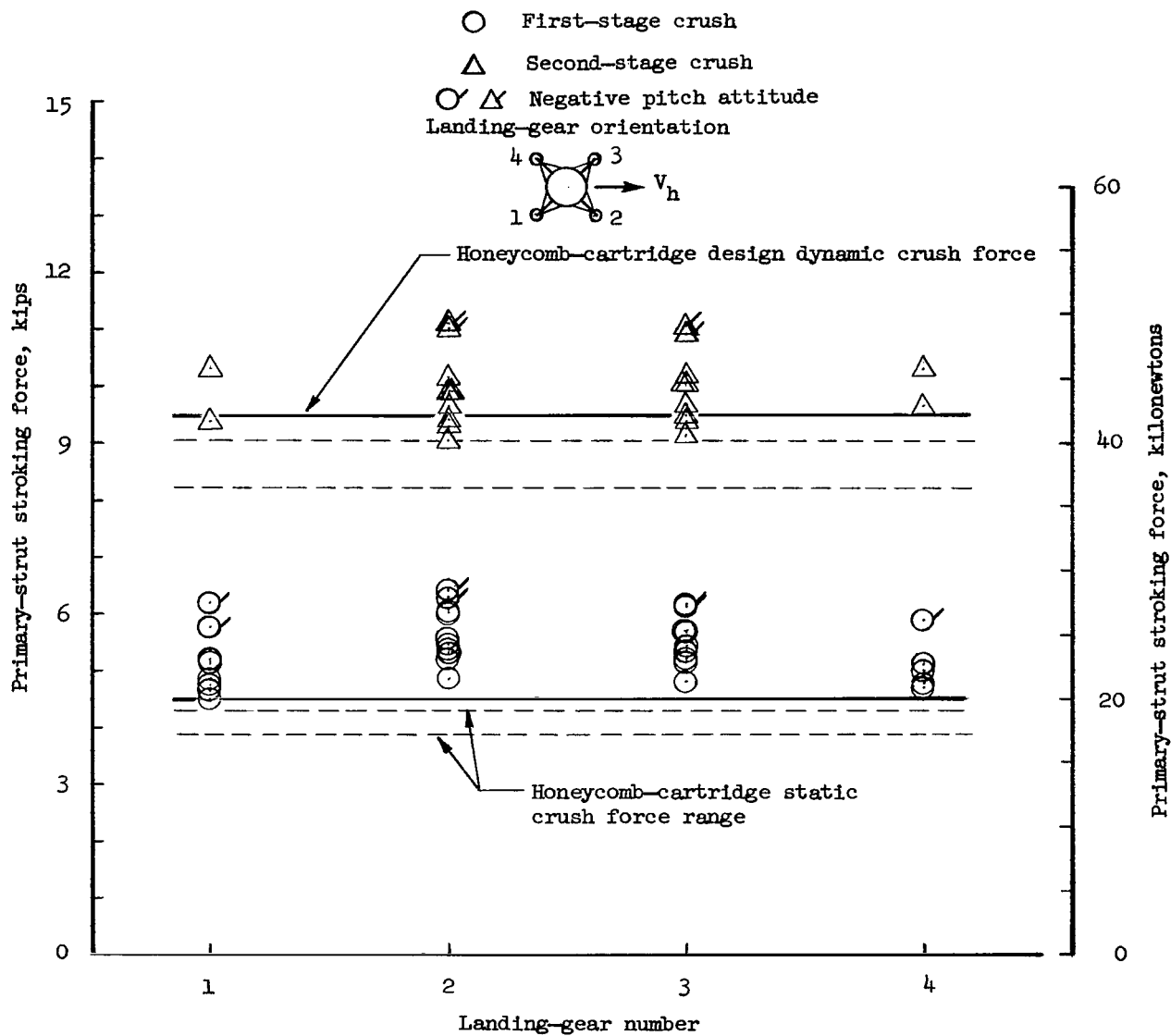
(a) 2-2 landing-gear orientation.

Figure 9.- Stroking forces measured on landing-gear primary struts during test vehicle landings.

31

(b) 1-2-1 landing gear orientation.

Figure 9.- Concluded.
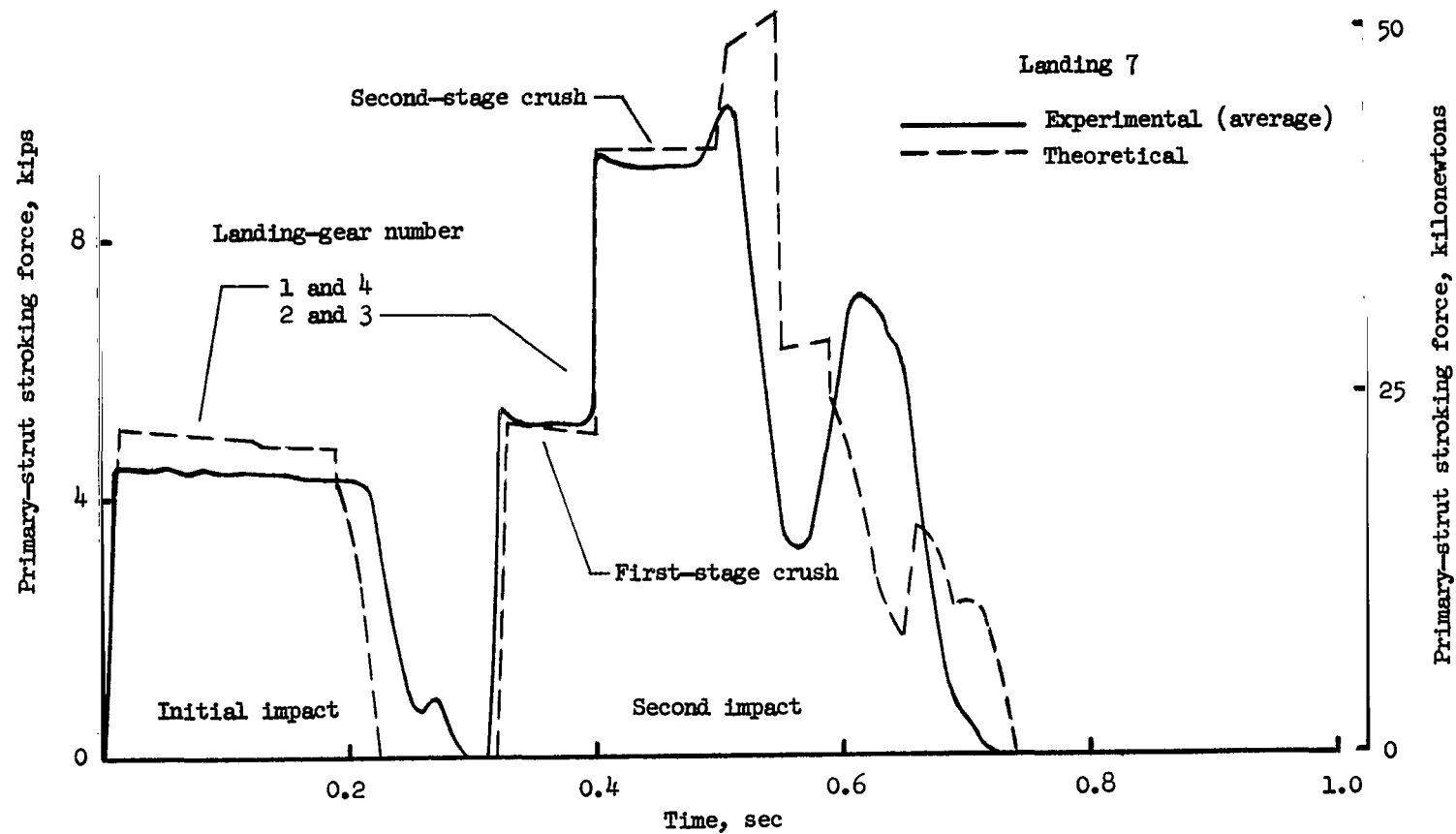
(a) 2-2 orientation; positive pitch attitude.

Figure 10.- Comparison of typical strut stroking-force time histories during landings of test vehicle and theoretical model.
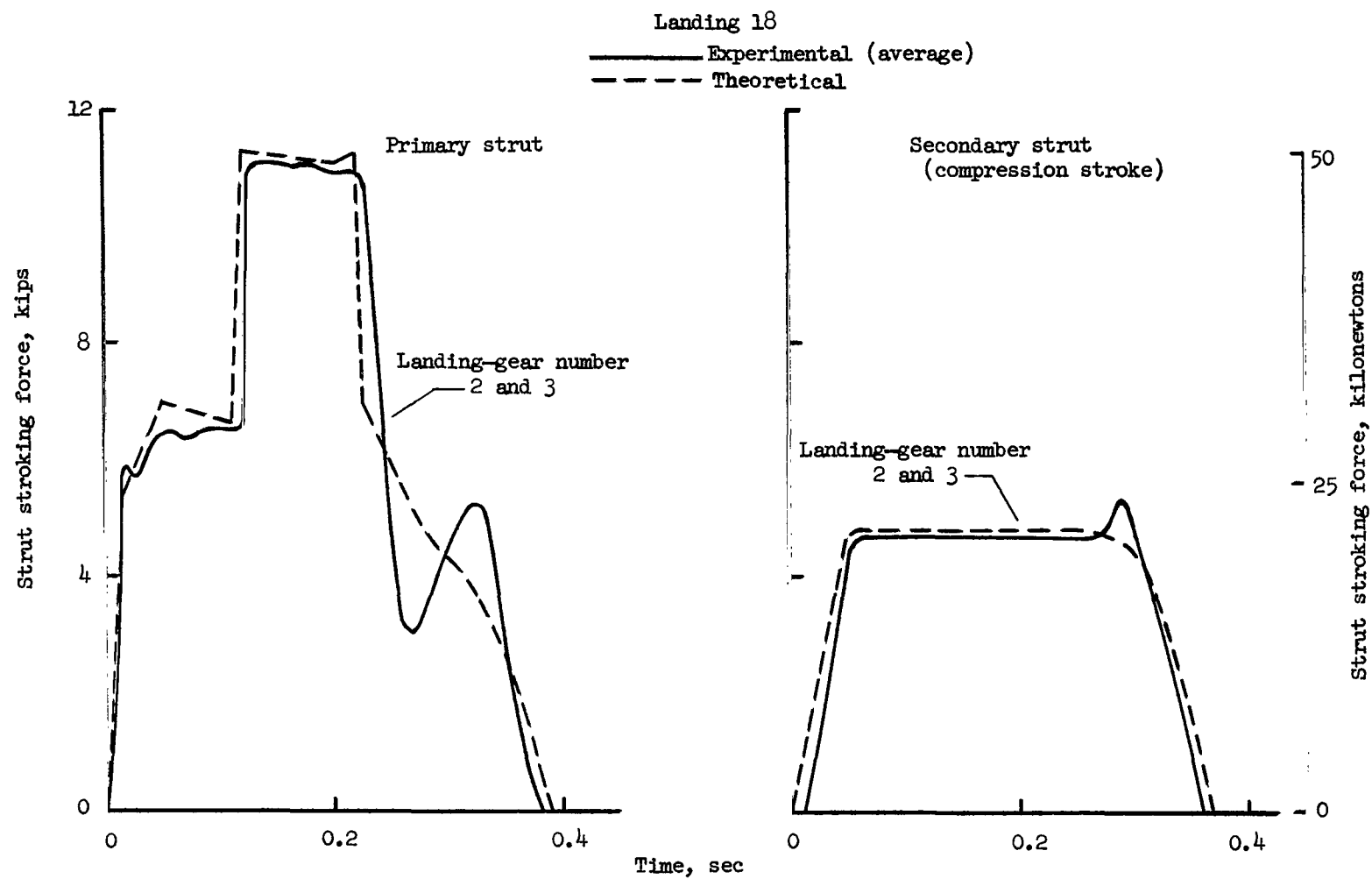
(b) 2-2 orientation; negative pitch attitude.

Figure 10.- Continued.
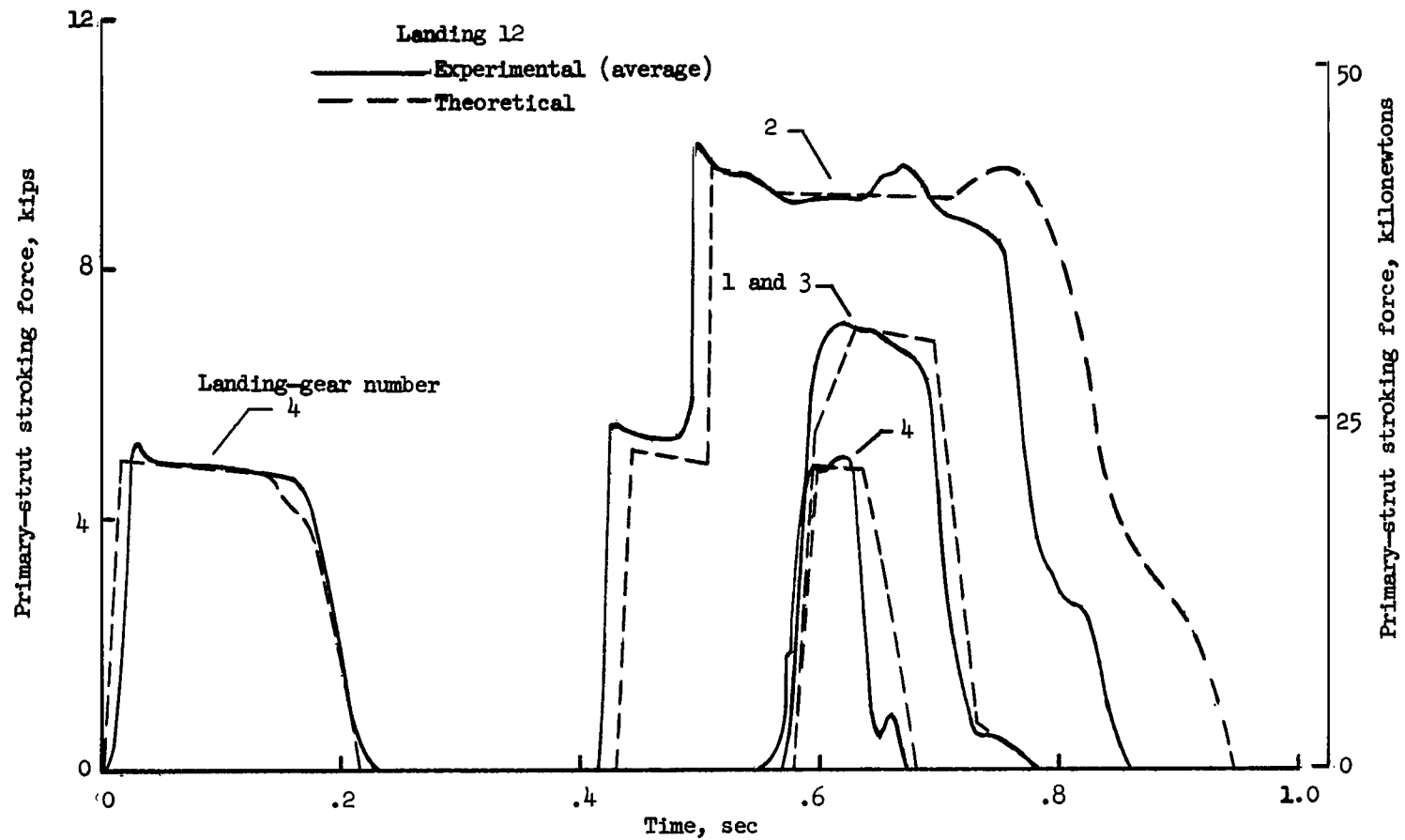
(c) 1-2-1 orientation; positive pitch attitude.

Figure 10.- Concluded.
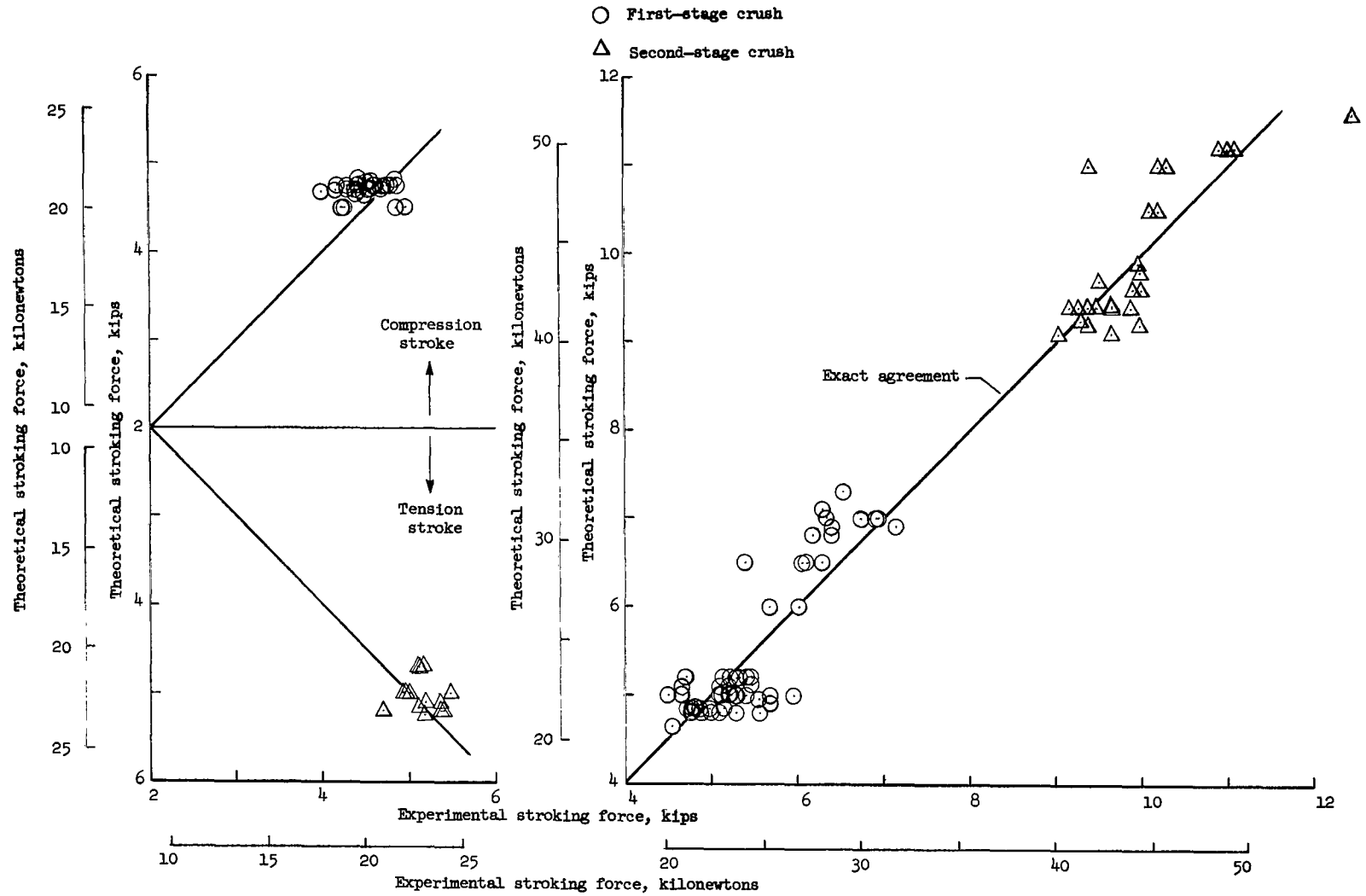
(a) Secondary struts.

(b) Primary struts.

Figure 11.- Comparison of stroking force of landing-gear struts during landings of test vehicle and theoretical model.
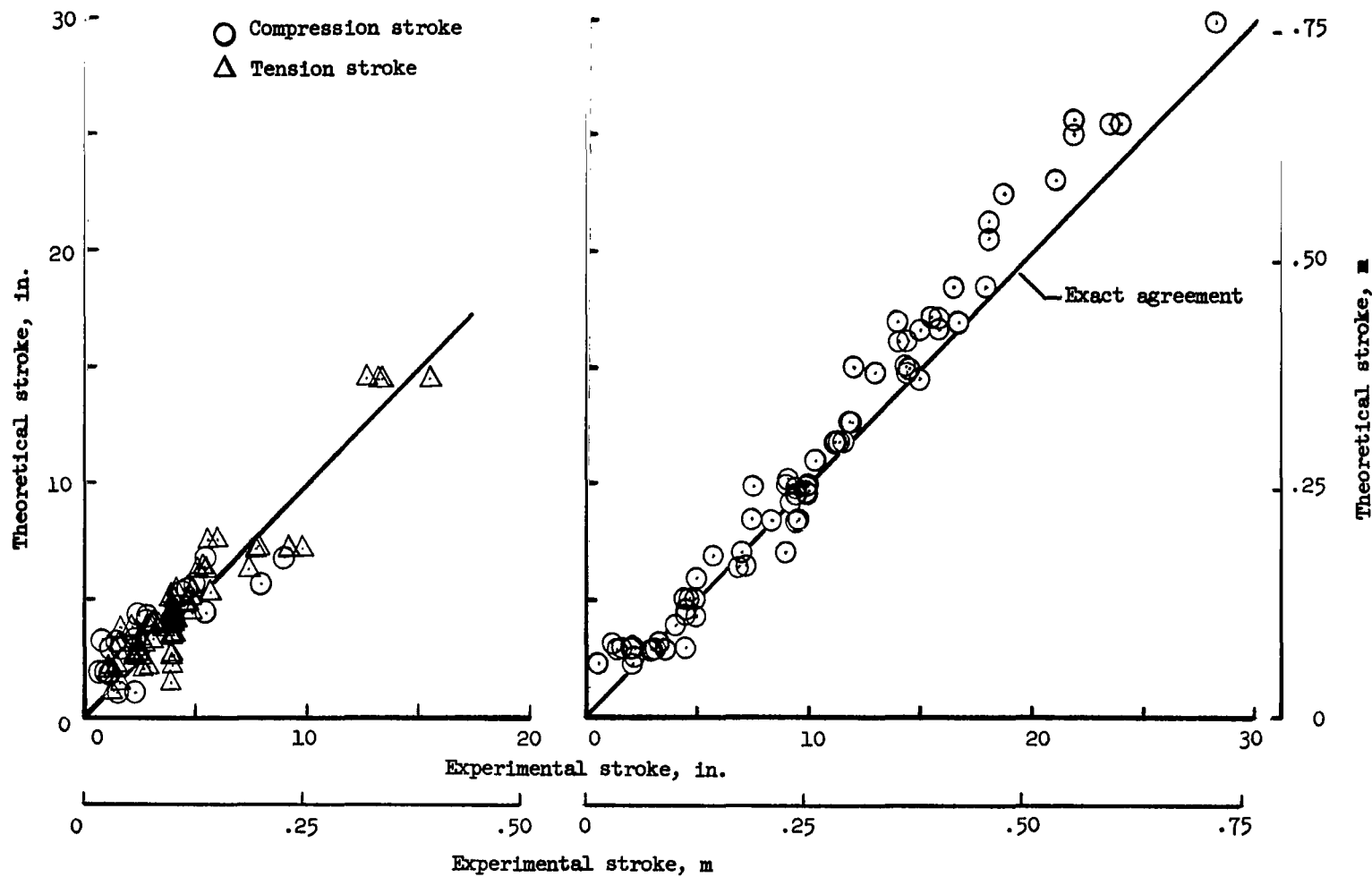
(a) Secondary struts.

(b) Primary struts.

Figure 12.- Comparison of total stroke of landing-gear struts during landings of test vehicle and theoretical model.
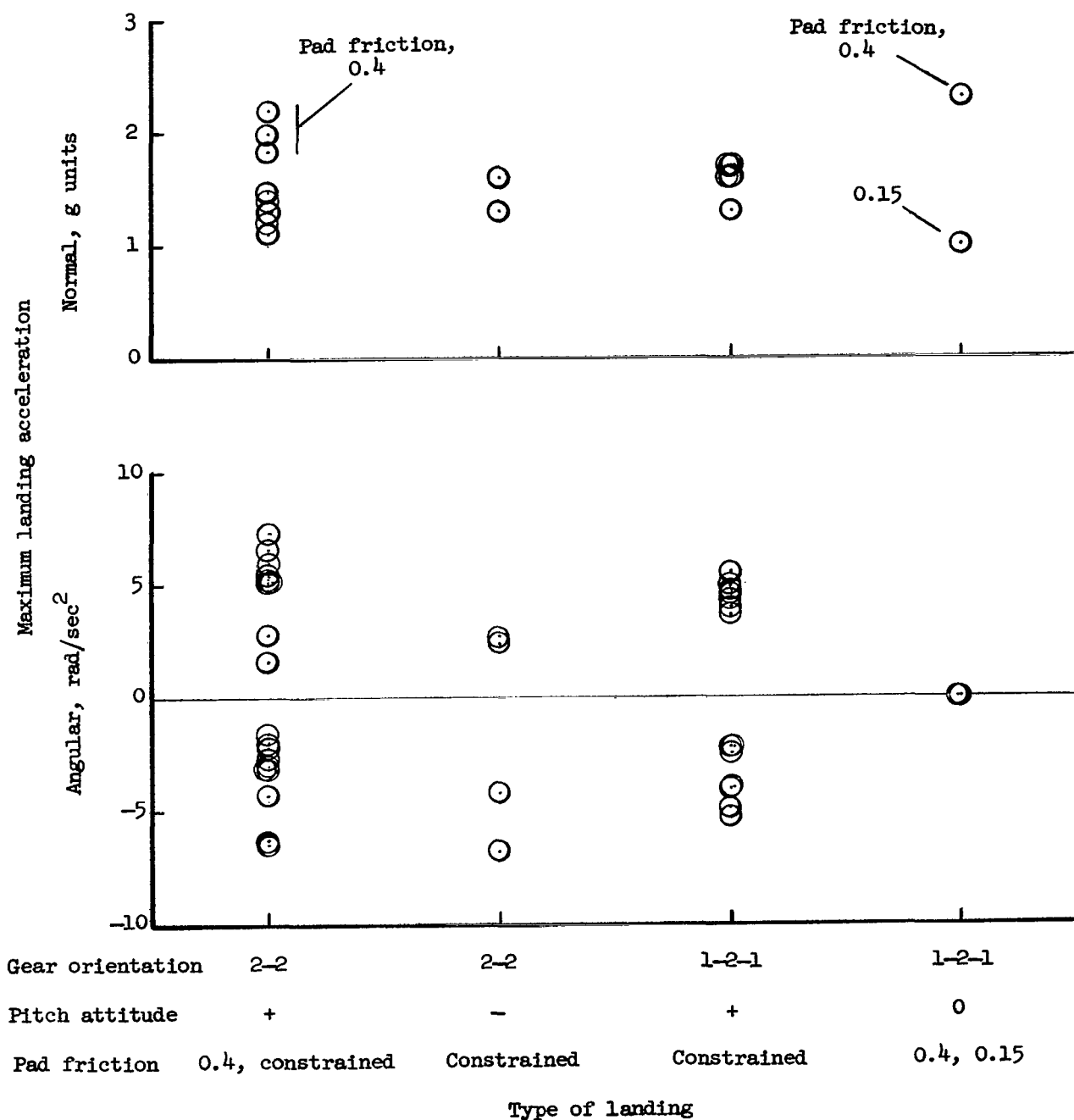
Figure 13.- Maximum center-of-gravity normal and angular accelerations measured on test vehicle during landings.

(a) Normal acceleration.

(b) Angular acceleration.
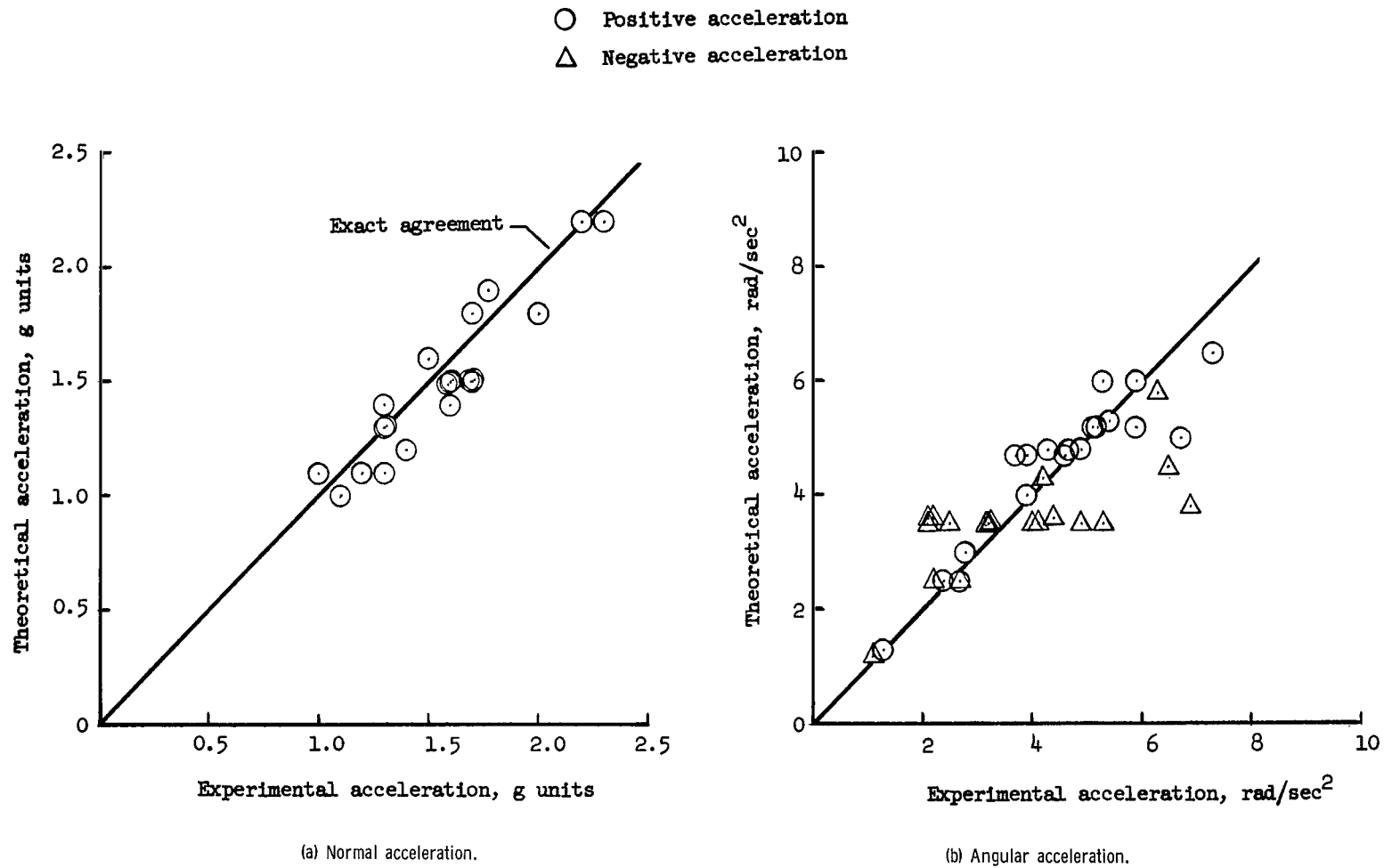
Figure 14.- Comparison of maximum normal and angular acceleration of center of gravity during landing of test vehicle and theoretical model.
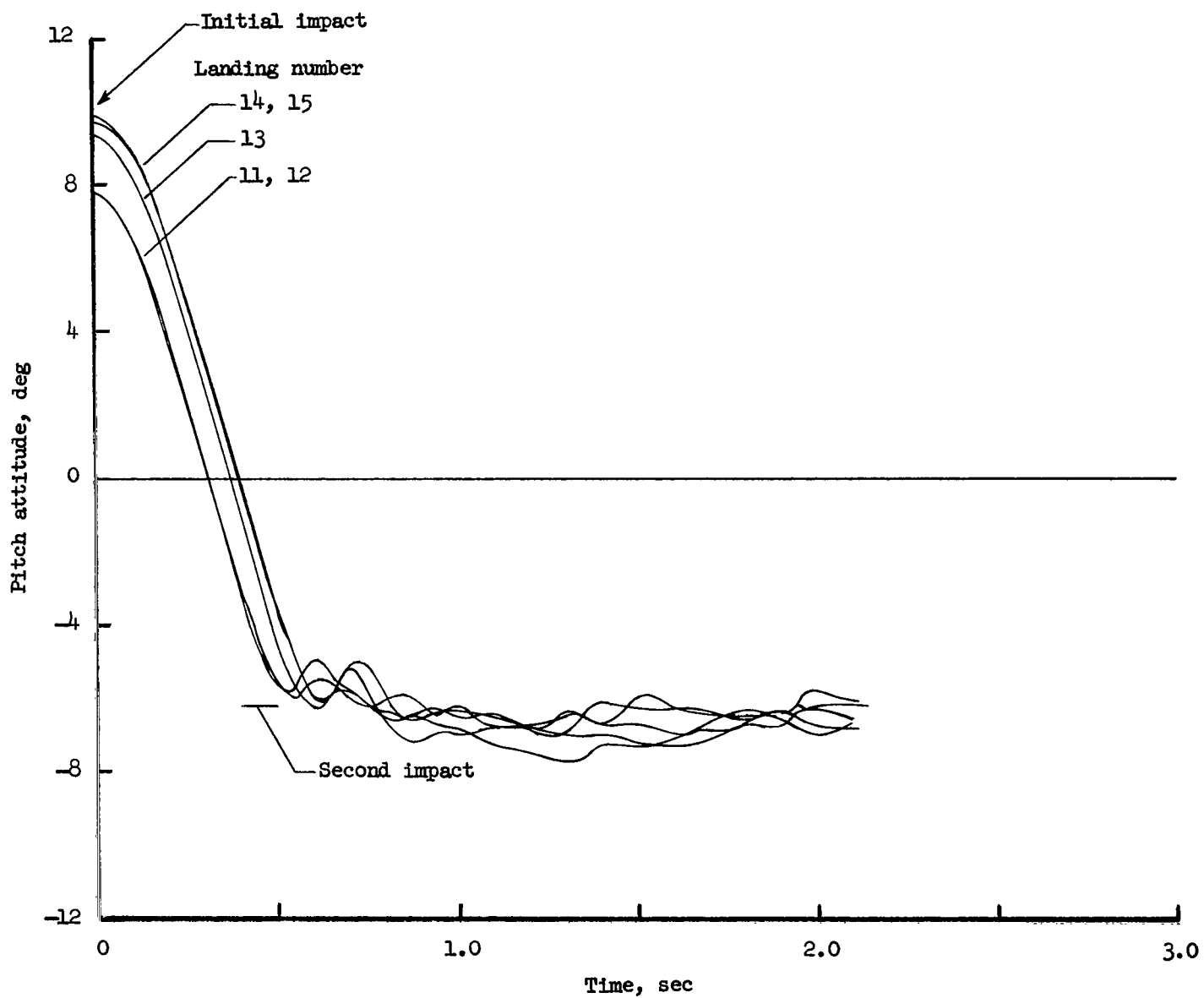
Figure 15.- Pitching motion during 1-2-1 landings of test vehicle.
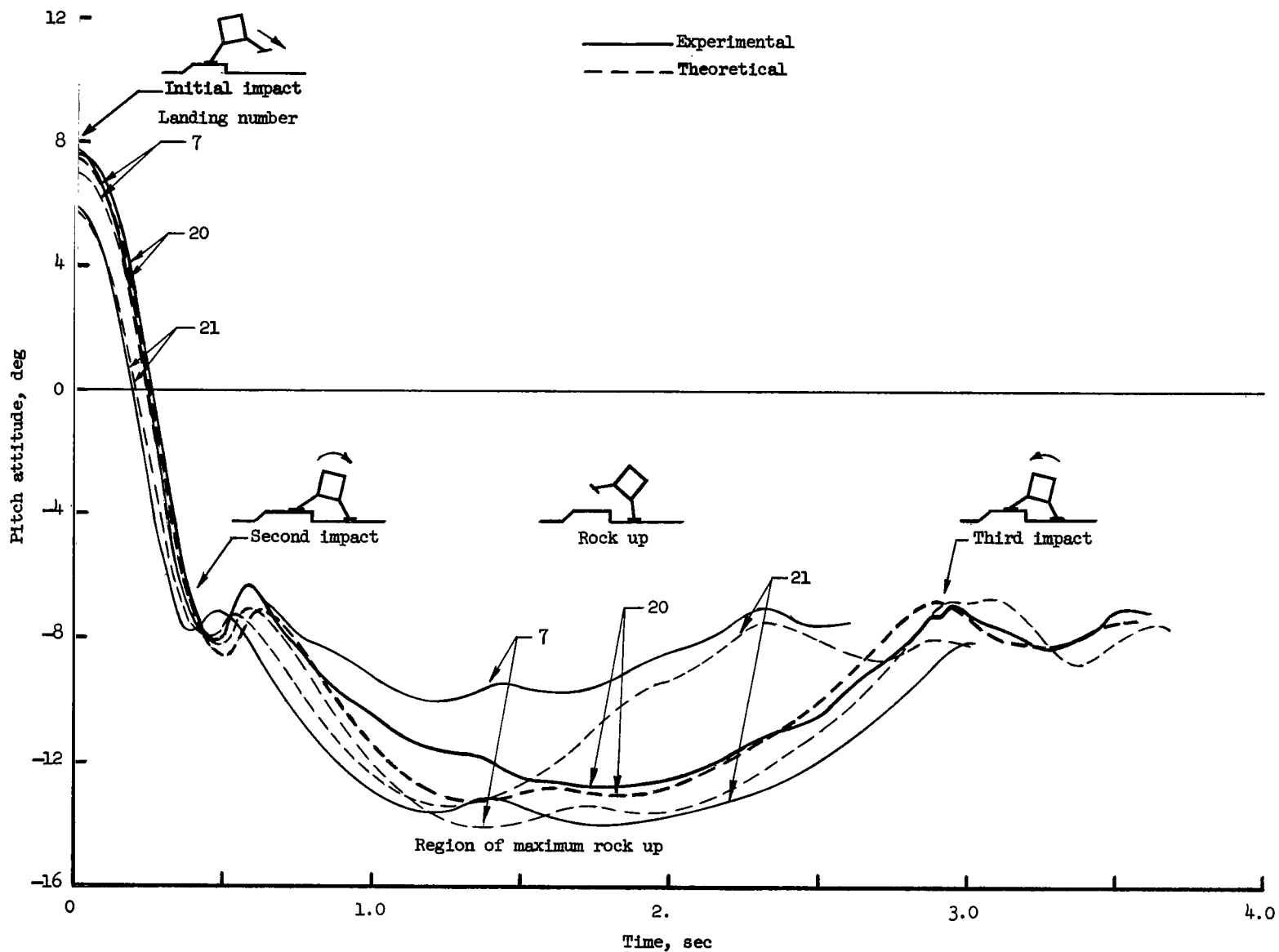
Figure 16.- Comparison of pitching motion during 2-2 landings of test vehicle and theoretical model.

A motion-picture film supplement L-1011 is available on loan. Requests will be filled in the order received. You will be notified of the approximate date scheduled.

The film (16 mm, 10 min, color, silent) shows test procedures and landings of the full-scale test vehicle.

Requests for the film should be addressed to:

NASA Langley Research Center
Att: Photographic Branch, Mail Stop 171
Langley Station
Hampton, Va. 23365

- - - - - - - - - - - - - - - - - - - CUT - - - - - - - - - - - - - - - - -

Date_____

Please send, on loan, copy of film supplement L-1011 to TN D-5029.

Name of organization _____

Street number _____

City and State _____ Zip code

Attention: Mr. _____

Title _____

"The aeronautical and space activities of the United States shall be conducted so as to contribute . . . to the expansion of human knowledge of phenomena in the atmosphere and space. The Administration shall provide for the widest practicable and appropriate dissemination of information concerning its activities and the results thereof."

— NATIONAL AERONAUTICS AND SPACE ACT OF 1958

NASA SCIENTIFIC AND TECHNICAL PUBLICATIONS

TECHNICAL REPORTS: Scientific and technical information considered important, complete, and a lasting contribution to existing knowledge.

TECHNICAL NOTES: Information less broad in scope but nevertheless of importance as a contribution to existing knowledge.

TECHNICAL MEMORANDUMS: Information receiving limited distribution because of preliminary data, security classification, or other reasons.

CONTRACTOR REPORTS: Scientific and technical information generated under a NASA contract or grant and considered an important contribution to existing knowledge.

TECHNICAL TRANSLATIONS: Information published in a foreign language considered to merit NASA distribution in English.

SPECIAL PUBLICATIONS: Information derived from or of value to NASA activities. Publications include conference proceedings, monographs, data compilations, handbooks, sourcebooks, and special bibliographies.

TECHNOLOGY UTILIZATION PUBLICATIONS: Information on technology used by NASA that may be of particular interest in commercial and other non-aerospace applications. Publications include Tech Briefs, Technology Utilization Reports and Notes, and Technology Surveys.

Details on the availability of these publications may be obtained from:

SCIENTIFIC AND TECHNICAL INFORMATION DIVISION

NATIONAL AERONAUTICS AND SPACE ADMINISTRATION
Washington, D.C. 20546